HHS Public Access

Author manuscript

Cell Rep. Author manuscript; available in PMC 2023 January 30.

Published in final edited form as:

Cell Rep. 2022 December 27; 41(13): 111894. doi:10.1016/j.celrep.2022.111894.

UCP2-dependent redox sensing in POMC neurons regulates feeding

Nal Ae Yoon[1], **Sungho Jin**[1], **Jung Dae Kim**[1], **Zhong Wu Liu**[2], **Qiushi Sun**[3], **Rebecca Cardone**[3], **Richard Kibbey**[3], **Sabrina Diano**[1,4,5,6,*]

[1]Institute of Human Nutrition, Columbia University Irving Medical Center, New York, NY 10032, USA

[2]Department of Comparative Medicine, Yale University School of Medicine, New Haven, CT 06520, USA

[3]Department of Internal Medicine, Yale University School of Medicine, New Haven, CT 06520, USA

[4]Department of Molecular Pharmacology and Therapeutics, Columbia University Irving Medical Center, New York, NY 10032, USA

[5]Department of Physiology and Cellular Biophysics, Columbia University Irving Medical Center, New York, NY 10032, USA

[6]Lead contact

SUMMARY

Paradoxically, glucose, the primary driver of satiety, activates a small population of anorexigenic pro-opiomelanocortin (POMC) neurons. Here, we show that lactate levels in the circulation and in the cerebrospinal fluid are elevated in the fed state and the addition of lactate to glucose activates the majority of POMC neurons while increasing cytosolic NADH generation, mitochondrial respiration, and extracellular pyruvate levels. Inhibition of lactate dehydrogenases diminishes mitochondrial respiration, NADH production, and POMC neuronal activity. However, inhibition of the mitochondrial pyruvate carrier has no effect. POMC-specific downregulation of *Ucp2* (*Ucp2*^{PomcKO}), a molecule regulated by fatty acid metabolism and shown to play a role as transporter in the malate-aspartate shuttle, abolishes lactate- and glucose-sensing of POMC neurons. *Ucp2*^{PomcKO} mice have impaired glucose metabolism and are prone to obesity on a high-fat diet. Altogether, our data show that lactate through redox signaling and blocking mitochondrial glucose utilization activates POMC neurons to regulate feeding and glucose metabolism.

*Correspondence: sabrina.diano@columbia.edu.

AUTHOR CONTRIBUTIONS

N.A.Y., R.K., and S.D. designed the experiments. N.A.Y., S.J., J.D.K., and Z.W.L. conducted and analyzed the experiments. Q.S. and R.C. performed and Q.S. and R.K. analyzed metabolomics. S.D. wrote the paper. N.A.Y., R.K., and S.D. reviewed and edited the paper.

DECLARATION OF INTERESTS

The authors declare no competing interests.

SUPPLEMENTAL INFORMATION

Supplemental information can be found online at https://doi.org/10.1016/j.celrep.2022.111894.

In brief

Yoon et al. show that lactate affects redox signaling in the hypothalamic anorexigenic POMC neurons and, by driving their activity, regulates feeding and peripheral glucose metabolism, a mechanism that depends on mitochondrial mechanisms related to uncoupling protein 2 (UCP2) and lipid utilization.

Graphical Abstract

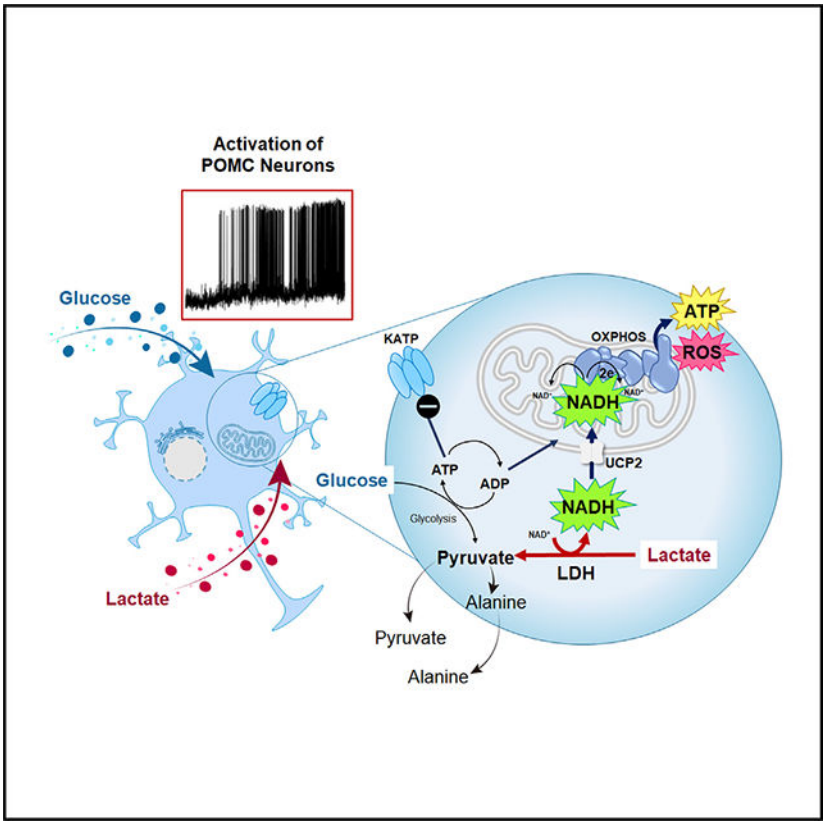

INTRODUCTION

Changes in metabolic states require the rapid and synergistic interaction between the brain and periphery to maintain homeostasis. Circulating factors produced and released by tissues, such as the liver, muscle, adipose, and pancreas, play fundamental roles in these processes. Hunger and satiety are controlled by food intake and related hormonal and metabolic adaptations. After a meal, an important signal that has been attributed to drive satiety is glucose,[1] which activates the anorexigenic pro-opiomelanocortin (POMC) neurons in the hypothalamus. Interestingly, only a subpopulation of POMC neurons shows activation by increased levels of glucose (for review, see Quarta et al.[2]).

In addition to glucose, lactate, the circulating redox indicator and glucose metabolite, has been shown to affect POMC activity. Indeed, lactate derived from either from the circulation or locally by glycolysis in glial cells (for review, see Magistretti and Allaman[3]) has been

shown to regulate neuronal function, including that of POMC neurons,[4] thus modulating peripheral glucose metabolism as well as feeding.[5–7]

Most recently, lactate has been postulated to play critical roles in inter-tissue communications during metabolic adaptations (for review, see Corkey and Deeney[8]). Changes in circulating lactate levels occur in response to feeding, when glucose levels are elevated, and fasting, when glucose levels decrease.[9–11] While administration of lactate has been shown to affect feeding and metabolism via the hypothalamus and POMC neurons,[5–7] the mechanism via which this process plays a role in physiological control of whole-body energy metabolism in association with glucose is ill-defined. We interrogated this question in relation to these first order satiety-promoting neurons of the brain, the arcuate nucleus POMC cells.

RESULTS

Lactate administration in presence of glucose more robustly activates POMC neurons

The anorexigenic POMC neurons are activated during positive energy balance such as the fed state. As glucose activates POMC neurons,[12,13] it has been thought that glucose is the main driver of POMC neuronal activation. However, in the fed state, other metabolites are elevated in the circulation and may affect POMC neuronal activity. As a recent report has shown that lactate, a circulating redox factor, induces activation of POMC neurons,[4] we measured lactate concentrations in fed versus fasted states in the circulation, as well as in the cerebroventricular fluid (CSF), of mice (Figure S1B). We found that in the fed state, when glucose levels are elevated compared with fasting (Figure S1A), both plasma and CSF lactate levels substantially increased compared with the fasted state (Figure S1B). Next, to determine the effect of lactate in the presence of physiological CNS glucose levels (2.5 mM), we performed POMC electrophysiological recording. Bath application of glucose alone (2.5 mM) induced a differential response in 77% of POMC neurons, of which 44% were activated (Figure 1A; 8 out of 18 POMC cells), while 33% were inhibited (6 cells out of 18 POMC cells). Membrane potential (Figure 1B) and frequency of action potentials of POMC neurons were not significantly affected by changes in glucose levels (Figure 1C). Addition of lactate (2.0 mM; Figure S1B)[14] to glucose (2.5 mM) triggered responses in the 82% of POMC neurons (Figure 1D). However, of these, a larger percentage, 67% (Figure 1D; 22 out of 35 POMC neurons), were excited, while only 15% were inhibited (5 cells out of 35 POMC cells), suggesting that the net impact of POMC activation was greater under glucose plus lactate (excitation/inhibition ratio 4.5:1) versus glucose alone (excitation/inhibition ratio 1.3:1). In contrast to the effect of glucose alone, lactate significantly decreased membrane potential (Figure 1E) and elevated frequency of action potentials (Figure 1F) of POMC neurons. Interestingly, pyruvate, the downstream metabolite of glycolysis, induced a lower response (Figure 1G; 36% of POMC neurons responsive) of POMC neurons, with only 27% (3 out of 11 cells) showing increased neuronal activity. Similar to the effect of glucose, membrane potential (Figure 1H) and frequency of action potentials (Figure 1I) of POMC neurons were not significantly affected by pyruvate. In addition, bath application of the inhibitor of the mitochondrial pyruvate carrier (MPC) 2-cyano-3-(1-phenyl-1H-indol-3-yl)-2-propenoic acid (UK5099; 5 μM) did

not significantly affect glucose-induced POMC membrane potential (Figure 1J), while bath application of oxamate (6 mM), the lactate dehydrogenase (LDH) inhibitor, significantly increased lactate-induced POMC membrane potential (Figure 1K), indicating that while lactate-to-pyruvate conversion plays a role in POMC neuronal activation, pyruvate transport into the mitochondria per se may not alter POMC function.

To further investigate the pronounced effect of lactate on POMC neuronal firing, we compared neuronal activity from glucose versus lactate on POMC *in vivo*. For that, freely moving *Pomc-CreER*^{T2} mice that selectively expressed the Ca^{2+} sensor GCaMP6s in POMC neurons (Figure 1L) were used for fiber photometric recordings. *In vivo* fiber photometry showed that compared with saline, glucose (2.5 mM) induced a small, but significant, increase in calcium fluxes in POMC neurons (Figures 1M and 1O). However, L-lactate (2 mM) induced a significantly stronger elevation in calcium fluxes in POMC neurons (Figures 1N and 1O). No significant effect of D-lactate (2 mM) on calcium fluxes was observed compared with saline (Figures 1N and 1O), indicating that lactate does not alter POMC activity by affecting the pH and the electrochemical properties.

In agreement with the electrophysiological and calcium recordings, cFos immunoreactivity in POMC neurons was significantly greater after intracerebroventricular (i.c.v.) administration of lactate than glucose (Figures S1C and S1D). Accordingly, i.c.v. lactate significantly decreased food intake in mice (*Ucp2*$^{+/+}$*;Pomc-CreER*^{T2}; Figure S1E).

Lactate differentially impacts mitochondria compared with glucose alone

We next examined the effects of basal glucose and glucose with pyruvate or lactate on the mitochondrial oxygen consumption rate of primary neuronal cultures derived from the medio-basal hypothalamus of *Pomc-CreER*^{T2}; tdTomato mice (Figures S2A and S2B). In these cultures, about 39% (39.3% [834/2,123]) of neurons expressed POMC (Figure S2B). We found that compared with glucose (2.5 mM; Figures 2B–2F) or glucose plus pyruvate (2 mM; Figures 2B–2F), glucose plus lactate (2 mM) significantly increased basal (Figure 2B) and maximal respiration (Figure 2C) as well as ATP production (Figure 2D). No differences on coupling efficiency (Figure 2E) or proton leak (Figure 2F) were observed, thus suggesting that the increased respiration is a function of increased ATP demand as a consequence of ATP hydrolysis from plasma membrane depolarization rather than increased mitochondrial leak. Furthermore, under physiological glucose levels, lactate dose-dependently increased mitochondrial basal (Figures S2C and S2D) and maximal respiration (Figures S2C and S2E) and ATP production (Figures S2C and S2F), whereas increasing glucose concentration did not affect the oxygen consumption rate (Figures S2G–S2J). Thus, these data indicate that lactate is the more physiologic enabler of depolarization and thus mitochondrial oxygen consumption in these POMC-enriched neuronal cultures.

In support of a role for lactate specifically augmenting mitochondrial function, oxamate, an LDH inhibitor, dose-dependently decreased lactate-induced mitochondrial basal (Figures S2K and S2L) and maximal respiration (Figures S2K and S2M) and lowered ATP production (Figures S2K and S2N), while UK5099, an inhibitor of pyruvate uptake by the MPC, did not change mitochondrial respiration under physiological glucose levels (Figures S2O–S2R). In addition, while UK5099 did not alter coupled or uncoupled mitochondrial

respiration in the presence of lactate (Figures 2G–2J), oxamate lowered basal (Figures 2G and 2H) and maximal respiration (Figures 2G and 2I) as well as ATP production (Figures 2G and 2J). Similarly, while oxamate also reduced glucose-induced mitochondrial basal (Figures 2K and 2L) and maximal respiration (Figures 2K and 2M) and ATP production (Figures 2K and 2N), UK5099 did not affect mitochondrial function (Figures 2K–2N). Altogether, these data suggest that while lactate oxidation by LDH plays a role in mitochondrial respiration, it does not perform this function through pyruvate utilization by the mitochondria. Thus, we next assessed the extracellular levels of pyruvate and alanine, a product of pyruvate metabolism. We found that lactate dose-dependently increased pyruvate (Figure 2O) and alanine concentrations (Figure 2P) in the culture media. Furthermore, in support of a role for LDH-mediated lactate oxidation in POMC neuronal function, we found greater levels of *Ldha* and *Ldhb* mRNA levels in POMC neurons of fed compared with fasted *Pomc-Cre*; RiboTag mice (Figures S3A–S3C). Altogether, these data indicate that LDH-mediated lactate metabolism plays a role in mitochondrial respiration in a pyruvate utilization-independent manner.

Lactate affects the redox state of POMC neurons

We have shown that under physiological glucose levels, lactate oxidation mediated by LDH is pivotal for mitochondrial function, and thus it may be part of a nutrient-sensing mechanism in POMC neurons. Because the function of LDH is to catalyze the reversible conversion of lactate to pyruvate with the reduction of NAD^+ to NADH,[15,16] this suggests the potential role of cytosolic NADH as redox-signaling molecules in POMC neurons. Next, we measured the cytosolic NADH:NAD^+ ratio by 2-photon microscopy using a fluorescent NADH sensor selectively expressed in POMC neurons (Figure 3A). A significant increase in NADH levels in POMC neurons was observed 15 min after the administration of lactate (2 mM) to hypothalamic slices (Figures 3B–3D). This increase in NADH generation was associated with increased reactive oxygen species (ROS) in POMC neurons (Figures 3E–3H; which are known to elevate POMC neuronal activity), consistent with the transfer of electrons to the electron transport chain (ETC).[17–19]

Cytosolic NADH donates electrons to the ETC via the malate-aspartate shuttle and/or the sn-glyceraldehyde-3-phosphate dehydrogenase shuttle, which can support oxidative phosphorylation. In support of such a lactate-NADH-shuttle mechanism regulating POMC neuronal function in the fed state, we found an increase in mRNA levels of genes associated with the malate/aspartate shuttle, including the cytoplasmic malate dehydrogenase 1 (*Mdh1*) (Figure S3D) and the cytoplasmic glutamic-oxaloacetic transaminase (*Got1*) (Figure S3E) in POMC neurons from fed *Pomc-Cre*; RiboTag mice compared with fasted *Pomc-Cre*; RiboTag mice.

We next measured mitochondrial respiration under different lactate (L):pyruvate (P) ratios (Figures 3I–3N) and found that decreasing the L:P ratio significantly decreased basal (Figures 3I and 3J) and maximal mitochondrial respiration (Figures 3I and 3K); ATP production (Figures 3I and 3L); and mitochondrial proton leak (Figures 3I and 3M) and increased coupling efficiency (Figures 3I and 3N). Taken together, these data indicate that

altering the equilibrium of the reaction catalyzed by LDH, which reflects the NADH:NAD^+ cytoplasmic redox state, negatively affects mitochondrial function.

Fatty acids stimulate mitochondrial function in POMC neurons

Our data showed that lactate-to-pyruvate conversion regulates the POMC redox state and drives oxidative phosphorylation, but it does not provide pyruvate as substrate for the tricarboxylic acid (TCA) cycle. To test whether alternative fuels, aside from redox shuttles, support respiration, we next added the fatty acid palmitic acid (PA) to primary mediobasal hypothalamic neuronal cultures. We found that basal glucose plus D-lactate did not stimulate respiration (Figures 3O–3S), while lactate and PA did (Figures 3O–3Q), but, importantly, without increasing proton leak (Figures 3O and 3S), ruling out an uncoupling effect. In agreement with this, significant increases in mRNA levels of genes involved in fatty acid oxidation,[20,21] such as uncoupling protein 2 (*Ucp2*) (Figure S3F) and carnitine palmitoyltransferase 1a (*Cpt1a*) (Figure S3G) and *Cpt1c* (Figure S3H), but not *Cpt1b* (Figure S3I), were observed in fed compared with fasted POMC neurons.

Deletion of *Ucp2* in POMC neurons diminishes glucose and lactate sensing

UCP2 is proposed to enable fatty acid metabolism.[22] In addition, it has been suggested to be involved in the malate-aspartate shuttle.[23,24] To assess the role of UCP2 in POMC cells, we next generated mice with selective and inducible deletion of *Ucp2* in POMC neurons ($Ucp2^{PomcKO}$) (Figures S4A and S4B). A significant decrease of *Ucp2* mRNA was observed in POMC neurons of $Ucp2^{PomcKO}$($Ucp2^{fl/f}$; $POMC\text{-}CreER^{T2}$; tdTomato; RiboTag) mice compared with controls ($Ucp2^{+/+}$; $POMC\text{-}CreER^{T2}$; tdTomato; RiboTag mice). No changes in the number of POMC neurons (Figures S4D and S4E) in the arcuate and in the intensity of POMC projections to the hypothalamic paraventricular nucleus were found between $Ucp2^{PomcKO}$ mice and controls (Figures S4F and S4G). Over 96% of POMC neurons expressed tdTomato in both control and $Ucp2^{PomcKO}$ mice (Figures S4H and S4I). No differences in pituitary *Pomc* mRNA levels (Figure S4J) and in circulating corticosterone levels (Figure S4K) were observed between $Ucp2^{PomcKO}$ and control mice.

Deletion of *Ucp2* in POMC neurons significantly decreased the number of POMC neurons that were excited by glucose (33%; 6 out of 18 POMC cells; Figures 4A–4C) and increased the number of non-responsive neurons to glucose (56%; 10 out of 18 POMC neurons; Figures 4A–4C). In response to lactate addition, there was a robust change in $Ucp2^{PomcKO}$ mice compared with controls (Figure 1A): only 7 out of 35 POMC neurons in $Ucp2^{PomcKO}$ mice were activated (20%; Figure 4D), while 60% of POMC neurons were non-responsive (21 out of 35 POMC neurons; Figure 4D). Accordingly, no changes in membrane potentials (Figure 4E) and frequency of action potentials (Figure 4F) were observed after lactate bath application in POMC neurons of hypothalamic sections from $Ucp2^{PomcKO}$ mice. i.c.v. lactate administration in $Ucp2^{PomcKO}$ mice decreased cFos immunoreactivity in POMC neurons and reduced POMC neuronal activation relative to control (Figures 4G–4I). In line with these changes, i.c.v. administration of lactate in $Ucp2^{PomcKO}$ mice did not alter food intake (Figure 4J) compared with vehicle injection in $Ucp2^{PomcKO}$ mice as it was shown to in control mice (Figure S1E).

Deletion of *Ucp2* in POMC neurons alters mitochondrial morphology, density, and function

Next, we analyzed mitochondrial morphology in fed $Ucp2^{PomcKO}$ and control mice (Figures S5A–S5E). $Ucp2^{PomcKO}$ mice showed a significant increase in mitochondrial number (Figure S5C) and a decrease in mitochondrial size (Figure S5D) with no changes in mitochondrial density (Figure S5E). These results indicate increased fission and/or decreased fusion of POMC mitochondria in fed $Ucp2^{PomcKO}$ mice, previously shown to play an inhibitory role in POMC function.[19,25] We then assessed mitochondrial respiration in primary mediobasal hypothalamic neuronal cultures from $Ucp2^{PomcKO}$ mice. While the addition of lactate in cultures derived from control mice significantly increased mitochondrial basal (Figures 5A and 5B) and maximal respiration (Figures 5A and 5C), as well as ATP production (Figures 5A and 5D), without affecting proton leak (Figure 5E), it did not increase the oxygen consumption rate in cultures derived from $Ucp2^{PomcKO}$ mice (Figures 5A–5D). No significant difference in glucose-induced mitochondrial respiration was observed between cultures derived from $Ucp2^{PomcKO}$ mice compared with those derived from controls (Figures 5A–5E). More importantly, no difference in proton leak was observed between control cultures and cultures derived from $Ucp2^{PomcKO}$ mice (Figure 5E) after either glucose or glucose plus lactate treatment, excluding a significant uncoupling activity of UCP2 in the cultures. Interestingly, and contrary to cultures derived from control mice (Figures 2K–2N) in which the inhibitor of MPC, UK5099, did not affect mitochondrial function, the addition of UK5099 (5 μM) to cultures from $Ucp2^{PomcKO}$ mice significantly decreased basal (Figures 5F and 5G) and maximal respiration (Figures 5F and 5H) and ATP production (Figures 5F and 5I) without altering proton leak (Figures 5F and 5J). These data, while indicating that UK5099 can indeed penetrate the cells and act at the mitochondrial level, suggest a role for pyruvate in stimulating mitochondrial function of $Ucp2^{PomcKO}$ mice. While glucose plus PA induced an increase in mitochondrial basal (Figures 5K and 5L) and maximal respiration (Figures 5K and 5M) and ATP production (Figures 5K and 5N) in cultures from control mice, it did not affect mitochondrial function in cultures from $Ucp2^{PomcKO}$ mice (Figures 5K–5O). Similar to the glucose and the glucose plus lactate treatments, PA administration did not alter proton leak in control and $Ucp2^{PomcKO}$ cultures (Figure 5O). Furthermore, UK5099 induced a significant hyperpolarization in POMC neurons of $Ucp2^{PomcKO}$ mice (Figure 5P). Altogether, our data indicate that UCP2 deletion does not impact uncoupled respiration and that its deletion induced a switch in mitochondrial fuel utilization.

Next, we assessed the NADH:NAD^+ ratio and found that lactate did not alter NADH levels in POMC neurons of $Ucp2^{PomcKO}$ mice (Figures 5Q–5S), suggesting that lactate in $Ucp2^{PomcKO}$ mice does not affect the cytosolic redox state of POMC neurons. In addition, a significant decrease in ROS in POMC neurons (Figures 5T–5V) was observed in $Ucp2^{PomcKO}$ compared with control mice, further supporting the lack of responsiveness of POMC neurons to changes in lactate levels in the absence of UCP2. In agreement with a role for lactate in regulating the POMC redox state, analysis of mitochondrial complexes showed a significant reduction of glutamate- and malate-stimulated respiration in cultures from $Ucp2^{PomcKO}$ mice compared with cultures derived from control mice (Figures 5W and 5X), while no significant differences were observed between complex II (Figure S5F) or the dicarboxylate carrier (DIC) and complex IV (Figure S5I). These data indicate that either

the malate-aspartate shuttle and/or complex 1 oxidation are impaired, and this is in line with the proposed role of UCP2 in the NADH-dependent mitochondrial function in POMC neurons. Finally, consistent with a disruption in the malate-aspartate shuttle and the redox state, metabolomics analysis showed a significant accumulation of metabolites (Figures S5J and S5K; Tables S1 and S2) involved in key pathways such as glycolysis and pentose cycles, glutamate metabolism, and the urea cycle in cultures derived from *Ucp2*^{PomcKO} mice compared with cultures derived from control mice treated with glucose (2.5 mM) and lactate (2 mM; Figures S5J and S5K; Tables S1 and S2).

Deletion of *Ucp2* in POMC neurons alters systemic glucose metabolism and promotes diet-induced obesity

We next assessed the metabolic phenotype of *Ucp2*^{PomcKO} mice. Compared with controls (*Ucp2*$^{+/+}$; *POMC-CreER*^{T2} or *Ucp2*$^{fl/f}$; *POMC-CreER*^{T2} with corn oil [vehicle]), no differences in body weight and composition were observed in both male (Figures S6A–S6C) and female (Figures S6D–S6F) *Ucp2*^{PomcKO} mice when fed a standard chow diet. However, we found that male *Ucp2*^{PomcKO} mice were glucose intolerant (Figures 6A and 6B) and insulin resistant compared with controls (Figures 6C and 6D). This was observed in females as well (Figures S6G–S6J).

We then analyzed the phenotypes of *Ucp2*^{PomcKO} mice and controls fed on a high-fat diet (HFD). A significantly increased body weight was observed in *Ucp2*^{PomcKO} mice starting at week 6 of HFD feeding compared with controls (Figure 6E). *Ucp2*^{PomcKO} mice displayed significantly higher fat mass but no changes in lean mass (Figure 6F). Differences in body weight (Figure 6E) and composition (Figure 6F) were associated with increased food intake (Figure 6G) and decreased locomotor activity (Figure 6H), specifically during the dark phase. In addition, a significantly lower energy expenditure (Figures 6I and 6J) and decreased O_2 consumption (Figure 6K) and CO_2 production (Figure 6L) in HFD-fed *Ucp2*^{PomcKO} mice were observed compared to control mice, while no significant difference in the respiratory exchange rate (RER) (Figure 6M) was observed.

DISCUSSION

Our study revealed a role for POMC neurons in detecting whole-body redox state by sensing and responding to changes in levels of lactate, a circulating redox buffer that equilibrates the NADH/NAD$^+$ ratio across cells and tissues. This mechanism requires mitochondrial UCP2 as a possible component of the malate-aspartate shuttle,[23,24] regulated by fatty acids,[26] that allows the translocation of electrons across the inner membrane of the mitochondria to enable oxidative phosphorylation.

Lactate derives from local glial cells (for review, see Magistretti and Allaman[3]) as well as from the circulation. Indeed, we have shown increased lactate levels in the circulation and in the CSF of fed mice compared with fasted mice. Furthermore, our data suggest that lactate acts as metabolite rather than electrolyte (affecting pH) in regulating POMC activity, as D-lactate did not affect mitochondrial function nor POMC activity. Interestingly, our results provide evidence that the role of lactate as metabolite is not to provide pyruvate as the major substrate for the TCA cycle and mitochondrial function.[27,28] In support of this, inhibition

of the MPC UK5099 did not affect lactate-stimulated mitochondrial respiration and ATP production, and lactate dose-dependently induced an increase in extracellular pyruvate levels, thus suggesting pyruvate as a by-product of lactate oxidation, non-responsible for lactate-induced stimulation of mitochondrial function. When lactate is oxidized to pyruvate, NAD^+ is reduced to NADH, which plays a critical role in the malate-aspartate shuttle and the sn-glyceraldehyde-3-phosphate dehydrogenase shuttle by donating electrons to the ETC so that ATP can be synthesized by mitochondria during oxidative phosphorylation. In support of a role for lactate-induced, NADH-mediated mitochondrial function and POMC neuronal activity, selective downregulation of UCP2 in POMC neurons impaired POMC neuronal activation, lactate-induced NADH generation, and mitochondrial function. UCP2, a mitochondrial protein whose function has been long debated, has been shown to be regulated by fatty acid and, most recently, has been suggested to play a role as transporter in the malate-aspartate shuttle.[23,24] Our data are in line with these findings as we found that malate-aspartate shuttle and/or complex 1 oxidation is impaired with the accumulation of metabolites in key pathways such as glycolysis, pentose and glutamate metabolism, and urea cycle in cultures from $Ucp2^{PomcKO}$ mice compared with cultures derived from control mice.

However, our data are in conflict with a previous published work[12] in which UCP2 was suggested to impair glucose sensing in POMC neurons. Several different approaches may be responsible for the divergent outcomes including our POMC-selective and -inducible UCP2 knockdown model versus the whole-body UCP2 knockout model and the acute pharmacological inhibition of UCP2 by a natural cross-linker of proteins, genipin, with unclear specificity to UCP2.[12]

A recent work by Li and collaborators[29] has shown that the blood-borne, exercise-inducible metabolite derived from lactate, N-lactoyl-phenilalanine (Lac-Phe), suppresses feeding and obesity,[29] thus raising the possibility that the effect of lactate in our study could be mediated, at least in part, by the peripheral conversion of lactate into Lac-Phe. However, our study, in which lactate was either centrally injected or added to the media of primary neuronal cultures, suggests that the effects observed may not be mediated by this metabolite. Future studies assessing the contribution of brain-derived Lac-Phe in regulating POMC function are warrented.

Interestingly, while lactate suppresses chow intake in mice, deletion of *Ucp2* in mice only shows body weight and feeding phenotypes when challenged by HFD. As in our study, mice fed on standard chow diet were studied up to 3 months of age; it is conceivable that with age, changes in body weight and feeding phenotypes may be displayed.

Our results suggest a working model of activation of POMC neurons during positive energy balance through their ability to sense a whole-body redox state. In the cytosol, glucose, by increasing ATP levels via glycolysis, induces closure of the K_{ATP} channels located on the POMC membrane,[1] resulting in membrane depolarization and a consequent decrease of the ATP/ADP ratio, an important driver of mitochondrial function. Then, lactate, derived either through the circulation or by the neighboring glial cells, by conversion to pyruvate, which is then secreted by the cell, reduces NAD^+ to NADH. Cytosolic NADH is then transported into the mitochondria, a mechanism requiring UCP2 as a possible component

of the malate-aspartate shuttle,[23,24] where, by donating electrons to the ETC via complex I, it enables the oxidative phosphorylation and ATP production needed to support POMC neuronal activity.

Limitations of the study

Our model leaves several open questions and limitations that will need to be addressed in the future. These include the identity of the metabolites that are utilized by the TCA cycle in POMC neurons during positive energy balance and the nature of our primary neuronal culture, which, although it had a high percentage of POMC-positive neurons, also contained other populations of neurons. It will ultimately be critical, but very challenging, to develop primary neuronal cultures composed exclusively by POMC neurons and to further evaluate our model *in vivo*.

STAR⋆METHODS

RESOURCE AVAILABILITY

Lead contact—Further information and requests for resources and reagents should be directed to and will be fulfilled by the lead contact, Sabrina Diano (Sabrina.diano@columbia.edu).

Material availability—All mouse strains generated in this study are available from the lead contact with a completed Materials Transfer Agreement.

Data and code availability

- The metabolomic data have been deposited at the NIH Common Fund's National Metabolics Data Repository (NMDR) website and are publicly available as of the date of publication. Accession numbers are listed in the key resources table. All data reported in this paper will be shared by the lead contact upon request.
- This paper does not report original code.
- Any additional information required to reanalyze the data reported in this paper is available from the lead contact upon request.

EXPERIMENTAL MODEL AND SUBJECT DETAILS

Mouse models and husbandry—All animal care and experimental procedures done in this study were approved by the Institutional Animal Care and Use Committee of Yale University (protocol # 10670) and Columbia University (Protocols # AC-AABI0565 and AC-AABH9564). Male and female mice were used in this study and housed in a temperature-controlled environment (22°C–24°C) with a 12-hr light and 12-hr dark (19:00 to 7:00) photoperiod. Animals were provided either a standard chow diet (SD) (2018; 18% calories from fat; Harlan Teklad) or a high fat diet (diet #93075; 45% fat; Harlan Teklad) and water *ad libitum* unless otherwise stated. All mice studied were of the same (mixed) background.

Generation of experimental mice with inducible deletion of *Ucp2* specifically in POMC neurons—We used the inducible Cre/loxP technology to generate mice in which UCP2 was selectively ablated in POMC neurons (*Ucp2*^{PomcKO} mice). First, mice expressing a tamoxifen-inducible Cre recombinase (*CreER*^{T2}) in cells expressing POMC (*Pomc-CreER*^{T2}) were crossed with Rosa26-lox-stop-lox-tdTomato (*Ai14*; cre-recombinase-dependent expression) mice (Ai14 reporter mice; stock #007914; The Jackson Laboratory) to label POMC-expressing cells. *Pomc-CreER*^{T2}; *Rosa26-lox-stop-lox*-tdTomato (*Pomc-CreER*^{T2}; tdTomato) mice have POMC-expressing cells with the expression of tdTomato by tamoxifen administration. No observation of POMC-tdTomato expression was found in the absence of tamoxifen administration, indicating that recombination was strictly dependent upon tamoxifen-induced Cre recombinase activation. The mice with *Pomc-CreER*^{T2}; tdTomato were then crossed with mice harboring conditional alleles *Ucp2* floxed (*Ucp2*$^{fl/fl}$; B6;129S-*Ucp2*$^{tm2.1Lowl/J}$, Stock# 022394; The Jackson Laboratory) to generated mice with inducible deletion of *Ucp2* specifically in POMC neurons (*Ucp2*^{PomcKO} mice). All animal experiments were conducted with the mice expressing *POMC-CreER*^{T2}. As control groups, *Ucp2*$^{fl/fl}$; Pomc-CreERT2 mice were injected with tamoxifen, and *Ucp2*$^{fl/fl}$; Pomc-CreERT2; tdTomato were mice injected with corn oil (vehicle), and *Ucp2*$^{fl/fl}$; Pomc-CreERT2; tdTomato mice were injected intraperitoneally (IP) with tamoxifen (0.1 mg/g BW for 5 consecutive days) starting at 5 weeks of age to induce mature-onset deletion of *Ucp2* in POMC neurons of *Ucp2*^{PomcKO} mice. However, because there were no differences between these two control groups, most of the experiments were performed using *Ucp2*$^{+/+}$; *Pomc-CreER*^{T2}; tdTomato mice injected with tamoxifen (to label POMC neurons with tdTomato expression) as a control group, unless otherwise stated. Body composition was measured *in vivo* by MRI (EchoMRI; Echo Medical Systems, Houston, TX) monthly at 10:00 AM. We performed transcriptomic profiling by using a ribosomal tagging strategy to analyze POMC neuron-specific mRNA expression *in vivo*. We crossed *Pomc-CreER*^{T2} mice[30] with *Rpl22* floxed (RiboTag, Stock# 029977, The Jackson Laboratories) mice to generate *Pomc-CreER*^{T2}; RiboTag mice, expressing a hemagglutinin A (HA)-tagged ribosomal protein in the POMC neurons upon tamoxifen injection.

Hypothalamic primary neuronal cell culture—Eight to ten neonatal (0 days old) pubs from either control or *Ucp2*^{PomcKO} mice derived from homozygous Cre-positive parents were used for hypothalamic primary neuronal cell culture. In brief, we carefully removed the brain's hypothalamus and placed it onto a small culture dish containing a small volume of Hibernate-A Medium (Cat# A1247501, Thermo Fisher Scientific). After digestion, the tissues dissociated to single cells with 6 mL of Hibernate-A Medium containing 2.5% of Trypsin-EDTA for 15 minutes at 37°C. Suspended cells were filtered (40 μm) and centrifuged for 5 min at 1000 rpm. The pellet was re-suspended and plated on XF96 cell culture microplates (Cat# 101085-004, Agilent Technologies) coated with poly-D-lysine (Cat# P6407, Sigma-Aldrich) at a density of 0.2×10^4 cells per well. Cells were cultured in Neurobasal-A medium (Cat# 10888022, Thermo Fisher Scientific) supplemented with 1% penicillin-streptomycin, 2% B-27 Supplement (Cat# 17504044, Thermo Fisher Scientific), and GlutaMAX-I (Cat# 35050061, Thermo Fisher Scientific), CultureOne supplement (Cat# A3320201, Thermo Fisher Scientific). For control culture, we used either *Ucp2*$^{fl/fl}$; *Pomc-CreER*^{T2}; tdTomato mice which neuronal cultures were treated with vehicle (0.03% ethanol

diluted in medium) or *Ucp2*$^{+/+}$; *Pomc-CreER*^{T2}; tdTomato mice which neuronal cultures were treated with 2 μM 4-hydroxytamoxifen (Cat# H7904, Sigma-Aldrich). After 10 days in culture, primary neuronal cells isolated from control and *Ucp2*^{PomcKO} mice were treated with 2 μM 4-hydroxytamoxifen for expression of a CreER recombinase. Primary neuronal cells were used for the measurement of mitochondria oxidation two days later.

METHOD DETAILS

Combined immunofluorescence and fluorescent *in situ* hybridization—To validate *Ucp2* deletion in *Ucp2*^{PomcKO} mice, we designed *Ucp2*-specific probe (corresponding to *Ucp2* exon 3 and 4, NM_011671 from NCBI gene bank). *Ucp2* probe was cloned into pBSK (+) Simple-Amp vector including T3 promoter for antisense RNA probe transcription (Molecular probes). Digoxygenin (DIG)-labeled antisense *Ucp2* probes were prepared by *in vitro* transcription using T3 RNA polymerase (Cat# P2083, Promega) and DIG RNA labeling Mix (Cat# 11277073910, Sigma-Aldrich) following the manufacturer's instructions and stored at −80°C. Once brains were removed from *Ucp2*^{PomcKO} and control mice, immediately put brains in liquid nitrogen. Frozen brains were colonially sectioned at 10 μm thicknesses using a cryostat and stored in −80°C until use. All solutions were prepared in diethylpyrocarbonate (DEPC)-treated water. First, we performed POMC staining using anti-rabbit POMC antibody (diluted 1:2,000 in 0.1 M PB, H-029-30, Phoenix Pharmaceuticals) and anti-rabbit Alexa 488 antibody (Cat# A21206, Thermo Fisher Scientific) at room temperature (RT) for 2 h. After washes with 0.1M PB, sections were further preceded for *in situ* hybridization. Briefly, sections were fixed with 3% paraformaldehyde (PFA), acetylated (2.7 mL of triethanolamine and 0.5 mL of acetic anhydride in 200 mL of DEPC water), dehydrated through a series of ethanol, and then hybridized with the DIG-labeled *Ucp2* antisense probes at 52°C for overnight. After hybridization and washes, sections were incubated with a peroxidase-conjugated anti-DIG antibody (diluted 1:1000 in TNB; 0.1 M Tris–HCl, pH 7.4, 0.05% Triton-X 100, 5 M NaCl, 2 mg/mL BSA in DEPC water, Cat# 11207733910, Sigma-Aldrich) at RT for 1.5 h followed by incubation for 30 min in Alexa Fluor 594 conjugated tyramide (diluted 1:200 in working solution, Cat# B40915, Thermo Fisher Scientific). TNT washing (3 × 10 min; 0.1 M Tris–HCl, pH 7.4, 0.15 M NaCl, 0.05% Triton-X-100 in DEPC water) was performed between each step. Sections were then coverslipped with Vectashield mounting solution (Cat# H-1000, Vector Laboratories) for microscopic examination.

POMC cell quantification in hypothalamic primary neuronal cell culture—To validate POMC cells percentage in cell derived from *Ucp2*^{PomcKO} and control mice, cells were treated with tamoxifen (to label POMC neurons with tdTomato expression) as a control group. After 48 h, cells were washed with pre-warmed 1x PBS and then incubated in 1 μM DAPI (Diluted in pre-warmed 1x PBS, Cat# P36962, Thermo Fisher Scientific) at RT for 5 min. After several washes with 1x PBS, coverslips were mounted on glass slides with a drop of Vectashield mounting medium (Cat# H-1000, Vector Laboratories) and five coverslips per group were then analyzed by capturing five random fields per coverslip observed cells on 20 x magnification by Fluorescence Microscope (Model BZ-X710, KEYENCE). For the quantitative analysis of cell numbers, tdTomato expressing cells in DAPI-stained were manually counted using ImageJ software.

Immunostaining—Mice were anesthetized and transcardially perfused with 0.9% saline with heparin, (10 mg/L, Cat# H3393, Sigma-Aldrich) following 4% PFA (diluted in 0.1 M PB). For double c-Fos and POMC immunostaining, brain sections were extensively washed in 0.1 M PB and blocked at RT for 60 min with blocking solution (contained 2% donkey serum, 0.2% Triton-X 100 in 0.1 M PB). The sections were incubated with rabbit anti-cFos antibody (diluted 1:2,000 in blocking solution, Cat# sc-52; Santa Cruz Biotechnology) 48 h at 4°C and then washed and incubated with a donkey anti-rabbit Alexa 488 antibody (diluted 1:100 in 0.1M PB, Cat# A21206 Thermo Fisher Scientific) for 2 h at RT. Sections were then washed and incubated with a donkey anti-rabbit IgG (diluted 1:40 in 0.1M PB, Cat# 711-005-152, Jackson ImmunoResearch) for 5 h at RT. Brain sections were then incubated with rabbit anti-POMC antibody (diluted 1:2,000 in blocking solution plus 2% goat serum, Cat# H-029-30, Phoenix Pharmaceuticals) overnight at RT. The following day, sections were washed and incubated with anti-rabbit Alexa Fluor 594 antibody (diluted 1:500 in 0.1 M PB, Cat# A32740, Thermo Fisher Scientific) for 2h at RT. To validate the expression of GCaMP6s Ca^{+} sensor in POMC neurons, brain sections were extensively washed in 0.1 M PB and incubated in anti-GFP antibody (Cat# ab13970, Abcam) overnight at 4°C (diluted 1:5000 in 0.1 M PB). After washes with 0.1 M PB and incubated in goat anti-chicken Alexa 488 antibody (diluted 1:200, Cat# A11039, Thermo Fisher Scientific) for 2h at RT. After several washes with 0.1 M PB, brain sections were mounted on glass slides and coverslipped with a drop of Vectashield mounting medium (Cat# H-1000, Vector Laboratories) and stored at 4°C until imaging.

Ribotag assays—14-week-old mice (two months after the last tamoxifen injection) were used, and the samples were prepared. Briefly, after mice were anesthetized with 5% of isoflurane and decapitated, the brains were rapidly dissected out. To carefully collect the hypothalamic ARC, brain tissues were sectioned in two-millimeter thick coronal sections containing mediobasal hypothalamus (MBH) in a brain matrix. The MBH ARC samples were collected under a stereomicroscope according to the brain atlas for appropriate regions and preventing differences in tissue weight. Four animals were pooled for each N. The MBH ARC samples from *Pomc-CreER^{T2}*; RiboTag mice were homogenized by supplemented homogenization buffer (HB-S: 50 mM Tris, pH 7.4, 100 mM KCl, 12 mM MgCl2, and 1% NP-40 supplemented with 1 mM DTT, 1 mg/mL heparin, 100 μg/mL cycloheximide, 200 U/mL RNasin Ribonuclease inhibitor, and protease inhibitor cocktail). Samples were then centrifuged at 10,000 rpm for 10 minutes at 4°C. Then, 50 μL of each supernatant was transferred to a new tube serving as input fraction (containing all mRNAs). To isolate polyribosomes, we performed immunoprecipitation of HA-tagged ribosome-bound mRNAs in POMC neurons. by utilizing anti-HA coated Magnetic Beads (100 μL/sample; Cat# 88836, Thermo Fisher Scientific). RNA was extracted using Qiagen RNeasy Plus Micro Kit (Cat# 74034, Qiagen) according to the protocol supplied by the manufacturer. cDNA was synthesized using High Capacity cDNA Reverse transcription Kit (Cat# 4368814, Thermo Fisher Scientific). All cDNA samples were amplified with selected target genes before qRT-PCR by the TaqMan PreAmp Master Mix (Cat# 4391128, Thermo Fisher Scientific) kit and a cocktail of the pooled TaqMan gene expression assay primers mix. Pre-amplified cDNA was diluted 1:20 in Tris EDTA buffer. The qRT-PCR experiment was performed by TaqMan gene expression assay primers (Applied Biosystems) in triplicates using Quant

Studio3 Real-Time PCR System (Applied Biosystem). All genes were normalized to *Actb*. The following primers were utilized: *Cpt1a*, Mm01231183_m1; *Cpt1b*, Mm00487191_g1; *Cpt1c*, Mm00463970_m1; *Cpt2*, Mm00487205_m1; *Pomc*, Mm00435874_m1; *Ldha*, Mm01612132_g1; *Ldhb*, Mm01267402_m1; *Got1*, Mm01195792_g1; *Mdh1*, Mm00485106_m1; *Ucp2*, Mm00627599_m1; *Actb*, Mm02619580-g1; *Actb*, 4352341E.

NADH measurement by two-photon fluorescence microscopy—For the expression of peredox protein in POMC neuron, pcDNA3.1-Peredox-mCherry-NLS (Cat# 32384, Addgene) plasmid was packaged into recombinant AAV serotype 2 (rAVV2-CMV-DIO-Peredox-mcherry-NLS) and produced at Vector Biolabs. 12 weeks old $Ucp2^{PomcKO}$ (n = 10–12 per group) and control mice were anesthetized with ketamine (100 mg/kg BW) and xylazine (10 mg/kg BW) and placed in a stereotaxic apparatus. The rAAV virus was injected into the ARC (coordinates, bregma: anterior-posterior, −1.6 mm; lateral, −0.3 mm; and dorsal-ventral, −5.85 mm) at a rate of 33 nL/min (~4.9×10^{12} GC/mL) for 15 min and secured to the skull with dental cement. After four weeks, mice were anesthetized with 5% of isoflurane, and decapitated, and the brain was then placed in a slicing solution (Contained 220 mM sucrose, 2.5 mM KCl, 1.23mM NaH2PO4, 26 mM NaHCO3, 1 mM CaCl2, 6 mM MgCl2, and 2.5 mM glucose, pH 7.3, with NaOH) at 4°C. After being amputated to a small tissue block, prepared coronal hypothalamic brain slices (~200 μm) with a Vibratome. Slices were immediately transferred to a chamber filled with artificial cerebrospinal fluid (aCSF) containing (in mM): NaCl 124, KCl 3, CaCl2 2, MgCl2 2, NaH2PO4 1.23, NaHCO3 26, glucose 3, pH 7.4 with NaOH at physiologic temperature (37°C). After preparation, slices were stored in a holding chamber with an oxygenated (with 5% CO_2 and 95% O_2) aCSF at RT for 30 min. In experiments, slices were incubated in aCSF containing either 2 mM L-lactate or vehicle for 15 min. Image stacks of the slices were acquired with a LaVision TriM Scope II (LaVision Biotec) microscope equipped with a Chameleon Vision II (Coherent) two-photon laser. A laser beam (at 940 nm for GFP and 1040 nm for RFP, respectively) was focused through a ×20 water immersion lens (N.A. 1.0; Olympus) and scanned with a field of view of 0.25 to 0.5 mm^2 at 600 Hz. Serial optical sections were acquired in 2 to 3 μm steps to image a total depth of ~100 μm of tissue in 5 min intervals.

Measurement of mitochondria oxidation—The oxygen consumption rate (OCR, which reflects mitochondrial oxidation) was measured using a microfluorimetric Seahorse Xfe96 Analyzer (Agilent Technologies) according to the protocol supplied by the manufacturer. Cell number per well was counted by fluorescently labeled nuclei from images captured by Cytation 1 to normalize OCR. Cells were starved with minimal substrate neurobasal-A medium (Cat# 10888022, Thermo Fisher Scientific) for 24 hours. The minimal substrate medium included 1% B-27 Supplement (Cat# 17504044, Thermo Fisher Scientific), 1 mM glutamine, and 2.5 or 0.5 mM of glucose. The day of the assay, 2 hs prior to the assay. Cells were washed with PBS and refilled with each Seahorse XF Base medium (assay medium, Cat# 102353-100, Agilent Technologies) containing with 2 mM L-glutamine (Cat# G8540, Sigma-Aldrich), 2.5 mM glucose (Cat# 7021, Sigma-Aldrich), 2 mM D-lactate (Cat# 71716, Sigma-Aldrich), 1, 2, 5, 10, 20 mM L-lactate (Cat# L7022, Sigma-Aldrich), 2 mM pyruvate (Cat# P2256, Sigma-Aldrich), 200 μM palmitate (Cat# P9767, Sigma-Aldrich), and 1, 2, 5, 10 μM of UK5099 (Cat# PZ0160, Sigma-Aldrich), 5,

10, 50, 100 mM of oxamate (Cat# O2751, Sigma-Aldrich). The plate was then incubated in a 37°C incubator without CO_2 for 2 h prior to the assay. During the assay, cells were exposed to compounds in the following order: For the Mito-stress assay Port A: 5 μM of oligomycin (Cat# 495455, Sigma-Aldrich), Port B: 10 μM of FCCP [carbonyl cyanide-p-(trifluoromethoxy) phenylhydrazone] (Cat# C2920, Sigma-Aldrich), and Port C: 10 μM of antimycin A (Cat# A8674, Sigma-Aldrich) and 5 μM of rotenone (Cat# R8875, Sigma-Aldrich) with 1 μM of DAPI. Wave 2.6.0 (Agilent Technologies software) software was used to normalize and analyze the parameters.

Electrophysiology—Eleven- to twelve-week-old fed male mice were used for recordings. After mice were anesthetized with isoflurane (5%) and decapitated, the brains were rapidly removed and immersed in an oxygenated cutting solution at 4°C. After being amputated to a small tissue block, coronal slices containing the hypothalamus (300 μm thick) were cut with a vibratome. After preparation, slices were stored in a holding chamber with an oxygenated (with 5% CO_2 and 95% O_2) aCSF. The slices were eventually transferred to a recording chamber perfused continuously with aCSF at 33°C at a rate of 2 mL/min after at least a 1 h recovery in the storage chamber. Perforated patch recording was performed in POMC-tdTomato neurons of the ARC under voltage and current clamp. The membrane and spontaneous action potential were recorded in POMC neurons under zero current clamp conditions. For POMC neuronal activation, baseline activity was recorded for at least 15 min. Slices were then perfused with 0.2 or 2.5 mM of glucose or 2 mM of lactate or 2 mM of pyruvate or 6 mM of oxamate or 5 μM of UK5099 diluted in aCSF for 3 min, followed by a washout. At the end of the perforated patch recordings, the membrane of every cell was ruptured and whole-cell patch recording was measured to check the current-voltage relationship. All data were sampled at 5 kHz, filtered at 2.4 kHz, and analyzed with an Apple Macintosh computer using AxoGraph X (AxoGraph Scientific). Statistics and plotting were performed with KaleidaGraph (Synergy Software, Inc.) and Igor Pro (WaveMetrics). The average firing rate was calculated in the last 2 min of each control period or treatment application. All the experiments were performed blindly to the electrophysiologist.

Intracerebroventricular (icv) cannulation and lactate administration—Two-month-old male mice were anesthetized with ketamine (100 mg/kg body mass) and xylazine (10 mg/kg) and placed in a stereotaxic apparatus (Stoelting). The cannula (33 gauge, P1 Technologies) was implanted into the right lateral ventricle (coordinates, bregma: anterior-posterior, −0.5 mm; lateral, −1.1 mm; and dorsal-ventral, −2.4 mm) and secured to the skull with dental cement. Animals were kept warm until they recovered from the anesthesia and then placed in individual cages. After surgery, a recovery period of 7 days was allowed before starting experiments. 1 week after surgery, individually housed 16-week-old mice (6 hours fasted) were icv injected with either saline or L-lactate (2 μL, 2 mM) at a rate of 0.4 μL/min for food intake experiment. Immediately after injection, mice were returned to their home cages, which contained a pre-weighed amount of food. The remaining food was measured at 1, 2, 4, 8, 16, and 24 hours time points. To measure POMC neuronal activation, mice were sacrificed and transcardially perfused with 0.9% saline with heparin followed by 4% at 1 h after L-lactate or saline injections (10:00 AM). Brains were then dissected and sectioned (50 μm) using a vibratome. Brain sections were processed for

cFos/POMC immunostaining as described above[19,34,35] Fluorescent images were captured with Fluorescence Microscope (Model BZ-X710, KEYENCE, Osaka, Japan). cFos/POMC positive cells were counted using ImageJ software. For fiber photometric recordings, individually housed 16-week-old (6 hours fasted) mice were IP injected with either saline or lactate (1 g/kg BW) at 1:00 PM. Immediately after injection, mice were returned to their home cages for measuring POMC calcium signaling using fiber photometry.

Stereotaxic surgery for fiber photometry and fiber photometric recordings— For fiber photometric recordings, we used recombinant AAV expressing cre-dependent GCaMP6s (pAAV.Syn.Flex.GCaMP6s.WPRE.SV40, Cat#100845, Addgene). Two-month-old male mice were deeply anesthetized with ketamine (100 mg/kg BW) and xylazine (10 mg/kg) and placed in a stereotaxic apparatus (Stoelting, Wood Dale, IL, USA). rAAV was stereotaxically injected unilaterally above the ARC of *Pomc-CreER^{T2}* mice (coordinates, bregma: anterior-posterior, −1.6 mm; lateral, −0.3 mm; and dorsal-ventral, −5.85 mm) at a rate of 33 nL/min (~2 × 10 GC/mL) for 15 min. During the same surgery a commercially available fiber-optic cannula (MFC_400/430-0.48_7 mm_MF1.25_FLT, Doric Lenses Inc.) was then implanted unilaterally into the ARC for *Pomc-CreER^{T2}* mice (coordinates, bregma: anterior-posterior, −1.6 mm; lateral, −0.3 mm; and dorsal-ventral, −5.8 mm) and secured to the skull with dental cement. Animals were kept warm until they recovered from the anesthesia and then placed in individual cages. After surgery, a recovery period of 7 days was allowed before starting experiments. 4 weeks before photometry recordings, 100 μL of 4-OH Tamoxifen (1 mg, Cat# H7904, Sigma-Aldrich) was IP injected into mice for Cre expression of POMC neurons. All fiber photometric recordings were performed with a rig using optical components from Doric lenses controlled by Tucker Davis Technologies (TDT) fiber photometry processor RZ10x. TDT Synapse software was used for data acquisition. Prior to experiments, the baseline POMC GCaMP6s signal was measured, and LED power was adjusted for each mouse to achieve approximately 150 mV for 465 nm (LX460) and 100 mV for 405 nm (LX405). All fiber photometry experiments were conducted after photobleaching (at least 1 hour) to minimize artifact signals. Prior to experimentation, all mice were habituated to the experimental cages and fiber handling was conducted for at least 3 days. A positive control test was performed to confirm the successful signal of the GCaMP6s. After 5 minutes of habituation stage, mice were icv injected with either saline, D-lactate (2 mM), glucose (2.5 mM) or L-lactate (2 mM) and POMC neuronal activity was monitored for 1 h. Data analysis was done using the modified MATLAB (TDTbin2mat) code provided by TDT.

ROS measurement—Reactive oxygen species (ROS) levels in POMC neurons were measured by injecting dihydroethidium (DHE, 1 mg/mL; Cat# D11347, Thermo Fisher Scientific) through the tail vein of *Ucp2$^{+/+}$*; *Pomc-CreER^{T2}* and *Ucp2$^{fl/fl}$*; *Pomc-CreER^{T2}* injected with tamoxifen (tdTomato negative), Two hours after the DHE injection, either glucose (2 g/kg BW) or lactate (1 g/kg BW) was injected, and one hour after the glucose or lactate injection, mice were anesthetized with isoflurane and transcardially perfused with 0.9% saline containing heparin (10 mg/L), followed by fresh 4% PFA. Brains were post-fixed overnight at 4°C and sliced to a thickness of 50 μm using a vibratome (#11000, PELCO easySlicer, TED PELLA Inc.) and coronal brain sections containing

the hypothalamic ARC were then washed and incubated with rabbit anti-POMC antibody (diluted 1:2,000 in 0.1 M PB, H-029-30, Phoenix Pharmaceuticals) at RT overnight and protected from the light. The following day, sections were washed and incubated with anti-rabbit Alexa 488 antibody (diluted 1:500 in 0.1 M PB, A21206, Life Technologies) for 2h at RT. After several washes with 0.1 M PB, brain sections were then mounted on glass slides and coverslipped with a drop of Vectashield mounting medium (Cat# H-1000, Vector Laboratories) and analyzed with a fluorescence microscope.

Glucose tolerance tests and insulin tolerance tests—Glucose tolerance tests (GTTs) were performed on animals that fasted for 16 h prior to testing from 18:00 to 10:00. After determination of basal blood glucose levels, each animal was injected with 2 g/kg glucose (Cat# G5765, Sigma-Aldrich). Blood glucose levels were measured by a glucometer (Contour 9556c, Bayer) at 15, 30, 60, and 120 min after glucose administration. Insulin tolerance tests (ITTs) were performed in *ad libitum* fed mice. After determining basal blood glucose levels, each animal received an IP injection of 0.75 U/kg insulin (Humulin R, Eli Lilly and Company). Blood glucose levels were measured by a glucometer at 15, 30, 60 and 120 min after insulin administration.

Indirect calorimetry system and body composition—Twelve-weeks-HFD-fed 5-month-old male mice were acclimated in metabolic chambers (TSE System-Core Metabolic Phenotyping Center, Yale University) for 3 days before the start of the recordings. Mice were continuously recorded for 2 days, with the following measurements taken every 30 min: food intake, locomotor activity (in the xy- and z-axes), and gas exchange (O_2 and CO_2; The TSE LabMaster System). Energy expenditure was calculated according to the manufacturer's guidelines (PhenoMaster Software, TSE System). The respiratory quotient was estimated by calculating the ratio of CO_2 production to O_2 consumption.

Values were adjusted by body weight to the power of 0.75 (kg–0.75) where mentioned. Body composition was measured *in vivo* by MRI (EchoMRI; Echo Medical Systems, Houston, TX).

Electron microscopy analysis—Five-month old male mice were deeply anesthetized and transcardially perfused with 0.9% saline containing heparin (10 mg/L), followed by a fresh fixative solution (4% paraformaldehyde, 15% picric acid, 0.1% glutaraldehyde in 0.1 M PB). Brain coronal sections were immunostained with rabbit anti-POMC antibody (diluted 1:2,000 in 0.1 M PB, H-029-30, Phoenix Pharmaceuticals) for POMC neurons. After several washes with 0.1 M PB, sections were incubated with biotinylated goat anti-rabbit IgG (diluted 1:250 in 0.1 M PB, Vector Laboratories) for 2h at RT, then rinsed in 0.1 M PB three times 10 min each time and incubated for 2h at RT with avidinbiotin–peroxidase (ABC; diluted 1:250 in 0.1 M PB; ABC Elite kit, Vector Laboratories). The immunoreaction was visualized with 3, 3-diaminobenzidine (DAB). Sections were then osmicated (1% osmium tetroxide) for 30 min, dehydrated through increasing ethanol concentrations (using 1% uranyl acetate in the 70% ethanol for 30 min), and flat-embedded in araldite between liquid release-coated slides (Electron Microscopy Sciences). After capsule embedding, blocks were trimmed. Ribbons of ultrathin serial sections were collected on Formvar-coated

single-slot grids and examined using a Philips CM-10 electron microscope. Mitochondria morphology in POMC neurons of fed and fasted mice were analyzed using ImageJ software.

Plasma, cerebrospinal fluid (CSF) and ARC L-lactate measurement—Mice plasma samples were collected from the tail vein using capillary blood collection (Microvette CB 300 K2 EDTA; Cat# 16.444.100, Sarstedt). Plasma from blood samples was obtained by centrifugation at 3,000 rpm for 20 min, at 4°C. For collecting CSF, mice were anesthetized with ketamine (100 mg/kg body mass) and xylazine (10 mg/kg) and placed in a stereotaxic apparatus. Glass capillary (Tip of the capillary; inner diameter 0.75 mm, outer diameter 1.0 mm; Cat# 1B100F-6, World precision instruments) was gently inserted into cisterna magna, then CSF was collected 5 to 10 μL. And mouse brains were dissected, and the ARC was snap-frozen in liquid nitrogen for 30 seconds. Then the isolated ARC samples were homogenized in lysis solution to precipitate protein. L-lactate levels were then measured using a commercially available L-lactate assay kit (Cat# ab65331, Abcam) according to the manufacturer's protocol.

Mass spectroscopy (see Tables S1 and S2)

Cell preparation: Cells cultured in 6-well plates were quickly washed once with ice cold 5 mM HEPES, then immediately quenched in 150ul/well ice cold quench buffer (20% methanol, 3 mM sodium fluoride, 0.1% formic acid, 1mM phenylalanine and 100uM EDTA). Each well was harvested using a cell lifter and immediately transferred to a pre-chilled 96-well plate on dry ice. Once completely frozen, cell lysates were lyophilized and stored in the −80°C freezer until the sample run. Lyophilized samples were prepared by resuspending in 50 μL water with D_4-taurine (50 μM) as an internal standard and 5 μL of the supernatant was injected for each analysis mode using high performance liquid chromatography (HPLC) into the 6600 Triple TOF LC-MS/MS mass spectrometer (Sciex).

Chromatography: Samples were run over two separate liquid chromatography columns in both positive and negative ion acquisition modes using the Thermo Scientific Hypercarb column (100 × 4.6 mm, 3 μm) and Phenomenex Kinetex F5 Core-shell LC column (100 × 2.1 mm, 2.6 μm). Separations were performed on the Hypercarb column with 1 mL/min linear gradients as indicated (Table 1). Mobile phase A: 15 mM ammonium formate, 0.03% acetyl acetone and 0.1% formic acid; mobile phase B: 60% ACN, 35% IPA, 15 mM ammonium formate and 0.1% formic acid. Column temperature was 50°C and autosampler temperature was 5°C.

For the Kinetex F5 column, separations were performed with 0.3 mL/min linear gradients as outlined (Table 2). Mobile phase A: 95% water, 5% acetonitrile and 0.1% formic acid; mobile phase B: 95% acetonitrile, 5% water and 0.1% formic acid. Column temperature was 30°C and autosampler temperature was 5°C.

QUANTIFICATION AND STATISTICAL ANALYSIS

Statistics—One way and Two-way ANOVA were used to determine the effect of the genotype and treatment with the Prism 9.03 software (GraphPad Software). For repeated measures analysis, ANOVA was used when values over different times were analyzed. When

only two groups were analyzed, statistical significance was determined by an unpaired two-tailed t-test. A value of $p < 0.05$ was considered statistically significant. All data is shown as mean ± SEM unless otherwise stated.

Fluorescent image analyses—Fluorescent images were captured with Fluorescence Microscope (Model BZ-X710, Keyence). For all immunohistochemistry (IHC) analyses, coronal brain sections were anatomically matched (ARC: between −1.46 and −1.94 mm from bregma, PVN: −0.82 and −0.94 mm from bregma) with the mouse brain atlas.[31] Both sides of the bilateral brain region (ARC and PVN) were analyzed per mouse. For each mouse, 3 hypothalamic level-matched per mouse were used to quantify c-Fos immunoreactive cells in all POMC immunostained cells observed in the ARC. The number of immunostained cells was counted manually using ImageJ software (1.47v, National Institutes of Health, http://rsbweb.nih.gov/ij/) by an unbiased observer. For area measurements and particle counting, region of interest (ROI) within fluorescence images was manually selected with the mouse brain atlas for ARC and PVN and was then measured by ImageJ.

Mass spectrometry analysis (see Tables S1 and S2)

Data procurement: Data were collected using an information-dependent analysis (IDA) workflow consisting of a TOF MS scan (200 msec) and a high-resolution IDA experiment (70 msec each) monitoring 10 candidate ions per cycle. Former target ions were excluded after 2 occurrences for 5 seconds and dynamic background subtraction was employed. The mass range for both TOF MS and IDA MS/MS scans was 60–1000 with the Kinetex F5 column and 70–1000 with the Hypercarb column. The ion source conditions were as follows; Ion spray voltage = 5000 V for positive mode and −4500 for negative mode, ion source gas 1 (GS1) = 50 psi, ion source gas 2 (GS2) = 50 psi, curtain gas (CUR) = 30 psi, temperature (TEM) = 400°C with F5 column and 500°C with Hypercarb column. Compound dependent parameters for the two modes were: declustering potential (DP) = 35 V, collision energy (CE) = 30 V, collision energy spread (CES) = 20 V.

Data processing: El-MAVEN software (Elucidata.io) was used for peak picking and curation from house built targeted and untargeted libraries. Targeted libraries were developed using a commercial standard kit of ~600 metabolites (IROA Technologies) in all 4 modes of analyses (2 LC columns in positive & negative modes) yielding reference data (molecular ions and retention times) with wide coverage of the endogenous metabolome. Untargeted libraries contained ~2,700 metabolites drawn from the KEGG database where the top 5 candidates with the highest intensity throughout a sample run for each metabolite were automatically curated. Data were normalized by the sum of all targeted metabolites within each sample in each mode and then log transformed. Sample quality was assessed using the internal standard D_4-taurine to identify any outliers to be excluded from the downstream analysis. Next, the normalized data from the two modes were merged. If a metabolite appeared in both modes, the one with the better signal was chosen. PCA, OPLS-DA, heat map and differential expression analyses on the merged targeted data were performed using the metabolomics application in Polly (polly.elucidata.io). Normal p values and log2FC data were uploaded in Shiny GATOM (https://artyomovlab.wustl.edu/shiny/

gatom/) to generate an optimized metabolic network displaying ~60 of the most changing and closely connected metabolites. The up-regulated and down-regulated metabolites in the *Ucp2*^{PomcKO} group were then used separately for pathway enrichment analysis in MetaboAnalyst (https://www.metaboanalyst.ca/).

Supplementary Material

Refer to Web version on PubMed Central for supplementary material.

ACKNOWLEDGMENTS

This work was supported by the National Institute of Health, United States, R01 DK097566, DK107293, DK120321 (to S.D.), R01DK127637 (R.K.), and 1S10OD030370-01A1.

INCLUSION AND DIVERSITY

We support inclusive, diverse, and equitable conduct of research.

REFERENCES

1. Ibrahim N, Bosch MA, Smart JL, Qiu J, Rubinstein M, Rønnekleiv OK, Low MJ, and Kelly MJ (2003). Hypothalamic proopiomelanocortin neurons are glucose responsive and express K(ATP) channels. Endocrinology 144, 1331–1340. 10.1210/en.2002-221033. [PubMed: 12639916]
2. Quarta C, Claret M, Zeltser LM, Williams KW, Yeo GSH, Tschöp MH, Diano S, Brüning JC, and Cota D (2021). POMC neuronal heterogeneity in energy balance and beyond: an integrated view. Nat. Metab. 3, 299–308. 10.1038/s42255-021-00345-3. [PubMed: 33633406]
3. Magistretti PJ, and Allaman I (2018). Lactate in the brain: from metabolic end-product to signalling molecule. Nat. Rev. Neurosci. 19, 235–249. 10.1038/nrn.2018.19. [PubMed: 29515192]
4. Lhomme T, Clasadonte J, Imbernon M, Fernandois D, Sauve F, Caron E, da Silva Lima N, Heras V, Martinez-Corral I, Mueller-Fielitz H, et al. (2021). Tanycytic networks mediate energy balance by feeding lactate to glucose-insensitive POMC neurons. J. Clin. Invest. 131, e140521. 10.1172/JCI140521. [PubMed: 34324439]
5. Lam TKT, Gutierrez-Juarez R, Pocai A, and Rossetti L (2005). Regulation of blood glucose by hypothalamic pyruvate metabolism. Science 309, 943–947. 10.1126/science.1112085. [PubMed: 16081739]
6. Lam CKL, Chari M, Wang PYT, and Lam TKT (2008). Central lactate metabolism regulates food intake. Am. J. Physiol. Endocrinol. Metab. 295, E491–E496. 10.1152/ajpendo.90481.2008. [PubMed: 18577696]
7. Kokorovic A, Cheung GWC, Rossetti L, and Lam TKT (2009). Hypothalamic sensing of circulating lactate regulates glucose production. J. Cell Mol. Med. 13, 4403–4408. 10.1111/j.1582-4934.2008.00596.x. [PubMed: 19040414]
8. Corkey BE, and Deeney JT (2020). The redox communication network as a regulator of metabolism. Front. Physiol. 11, 567796. 10.3389/fphys.2020.567796. [PubMed: 33178037]
9. Williamson DH, Lund P, and Krebs HA (1967). The redox state of free nicotinamide-adenine dinucleotide in the cytoplasm and mitochondria of rat liver. Biochem. J. 103, 514–527. 10.1042/bj1030514. [PubMed: 4291787]
10. Williamson JR, and Corkey BE (1969). Assays of intermediates of the citric acid cycle and related compounds by fluorometric enzyme methods. In Citric Acid Cycle, Volume 13, Lowenstein JM, ed. (Methods in Enzymology), pp. 434–513.
11. Williamson JR, and Corkey BE (1979). Assay of citric acid cycle intermediates and related compounds—update with tissue metabolite levels and Intracellular Distribution. In Biomembranes Part F: Bioenergetics: Oxidative Phosphorylation, Volume 55, Sidney Fleischer LP, ed. (Methods in Enzymology), pp. 200–222.

12. Parton LE, Ye CP, Coppari R, Enriori PJ, Choi B, Zhang CY, Xu C, Vianna CR, Balthasar N, Lee CE, et al. (2007). Glucose sensing by POMC neurons regulates glucose homeostasis and is impaired in obesity. Nature 449, 228–232. 10.1038/nature06098. [PubMed: 17728716]

13. Claret M, Smith MA, Batterham RL, Selman C, Choudhury AI, Fryer LGD, Clements M, Al-Qassab H, Heffron H, Xu AW, et al. (2007). AMPK is essential for energy homeostasis regulation and glucose sensing by POMC and AgRP neurons. J. Clin. Invest. 117, 2325–2336. 10.1172/JCI31516. [PubMed: 17671657]

14. Leen WG, Willemsen MA, Wevers RA, and Verbeek MM (2012). Cerebrospinal fluid glucose and lactate: age-specific reference values and implications for clinical practice. PLoS One 7, e42745. 10.1371/journal.pone.0042745. [PubMed: 22880096]

15. Holmes RS, and Goldberg E (2009). Computational analyses of mammalian lactate dehydrogenases: human, mouse, opossum and platypus LDHs. Comput. Biol. Chem. 33, 379–385. 10.1016/j.compbiolchem.2009.07.006. [PubMed: 19679512]

16. Wilks HM, Hart KW, Feeney R, Dunn CR, Muirhead H, Chia WN, Barstow DA, Atkinson T, Clarke AR, and Holbrook JJ (1988). A specific, highly active malate dehydrogenase by redesign of a lactate dehydrogenase framework. Science 242, 1541–1544. 10.1126/science.3201242. [PubMed: 3201242]

17. Diano S, Liu ZW, Jeong JK, Dietrich MO, Ruan HB, Kim E, Suyama S, Kelly K, Gyengesi E, Arbiser JL, et al. (2011). Peroxisome proliferation-associated control of reactive oxygen species sets melanocortin tone and feeding in diet-induced obesity. Nat. Med. 17, 1121–1127. 10.1038/nm.2421. [PubMed: 21873987]

18. Long L, Toda C, Jeong JK, Horvath TL, and Diano S (2014). PPAR-gamma ablation sensitizes proopiomelanocortin neurons to leptin during high-fat feeding. J. Clin. Invest. 124, 4017–4027. 10.1172/JCI76220. [PubMed: 25083994]

19. Santoro A, Campolo M, Liu C, Sesaki H, Meli R, Liu ZW, Kim JD, and Diano S (2017). DRP1 suppresses leptin and glucose sensing of POMC neurons. Cell Metab. 25, 647–660. 10.1016/j.cmet.2017.01.003. [PubMed: 28190775]

20. Andrews ZB, Liu ZW, Walllingford N, Erion DM, Borok E, Friedman JM, Tschöp MH, Shanabrough M, Cline G, Shulman GI, et al. (2008). UCP2 mediates ghrelin's action on NPY/AgRP neurons by lowering free radicals. Nature 454, 846–851. 10.1038/nature07181. [PubMed: 18668043]

21. Jin S, Yoon NA, Liu ZW, Song JE, Horvath TL, Kim JD, and Diano S (2021). Drp1 is required for AgRP neuronal activity and feeding. Elife 10, e64351. 10.7554/eLife.64351. [PubMed: 33689681]

22. Echtay KS, Roussel D, St-Pierre J, Jekabsons MB, Cadenas S, Stuart JA, Harper JA, Roebuck SJ, Morrison A, Pickering S, et al. (2002). Superoxide activates mitochondrial uncoupling proteins. Nature 415, 96–99. 10.1038/415096a. [PubMed: 11780125]

23. Vozza A, Parisi G, De Leonardis F, Lasorsa FM, Castegna A, Amorese D, Marmo R, Calcagnile VM, Palmieri L, Ricquier D, et al. (2014). UCP2 transports C4 metabolites out of mitochondria, regulating glucose and glutamine oxidation. Proc. Natl. Acad. Sci. USA 111, 960–965. 10.1073/pnas.1317400111. [PubMed: 24395786]

24. Raho S, Capobianco L, Malivindi R, Vozza A, Piazzolla C, De Leonardis F, Gorgoglione R, Scarcia P, Pezzuto F, Agrimi G, et al. (2020). KRAS-regulated glutamine metabolism requires UCP2-mediated aspartate transport to support pancreatic cancer growth. Nat. Metab. 2, 1373–1381. 10.1038/s42255-020-00315-1. [PubMed: 33230296]

25. Ramírez S, Gómez-Valadés AG, Schneeberger M, Varela L, Haddad-Tóvolli R, Altirriba J, Noguera E, Drougard A, Flores-Martínez Á., Imbernón M, et al. (2017). Mitochondrial dynamics mediated by mitofusin 1 is required for POMC neuron glucose-sensing and insulin release control. Cell Metab. 25, 1390–1399.e6. 10.1016/j.cmet.2017.05.010. [PubMed: 28591639]

26. Berardi MJ, and Chou JJ (2014). Fatty acid flippase activity of UCP2 is essential for its proton transport in mitochondria. Cell Metab. 20, 541–552. 10.1016/j.cmet.2014.07.004. [PubMed: 25127353]

27. Barros LF (2013). Metabolic signaling by lactate in the brain. Trends Neurosci. 36, 396–404. 10.1016/j.tins.2013.04.002. [PubMed: 23639382]

28. Pellerin L, Pellegri G, Bittar PG, Charnay Y, Bouras C, Martin JL, Stella N, and Magistretti PJ (1998). Evidence supporting the existence of an activity-dependent astrocyte-neuron lactate shuttle. Dev. Neurosci. 20, 291–299. 10.1159/000017324. [PubMed: 9778565]

29. Li VL, He Y, Contrepois K, Liu H, Kim JT, Wiggenhorn AL, Tanzo JT, Tung ASH, Lyu X, Zushin PJH, et al. (2022). An exercise-inducible metabolite that suppresses feeding and obesity. Nature 606, 785–790. 10.1038/s41586-022-04828-5. [PubMed: 35705806]

30. Berglund ED, Liu C, Sohn JW, Liu T, Kim MH, Lee CE, Vianna CR, Williams KW, Xu Y, and Elmquist JK (2013). Serotonin 2C receptors in pro-opiomelanocortin neurons regulate energy and glucose homeostasis. J. Clin. Invest. 123, 5061–5070. 10.1172/JCI70338. [PubMed: 24177424]

31. Franklin K, and Paxinos G (2019). Paxinos and Franklin's the Mouse Brain in Stereotaxic Coordinates, Compact (Academic Press).

Highlights

- The redox metabolite, lactate, plays a role in regulating POMC neuronal activity
- Redox sensing by POMC neurons regulates POMC activity through mitochondrial oxidation
- UCP2-dependent redox sensing in POMC neurons regulates food intake

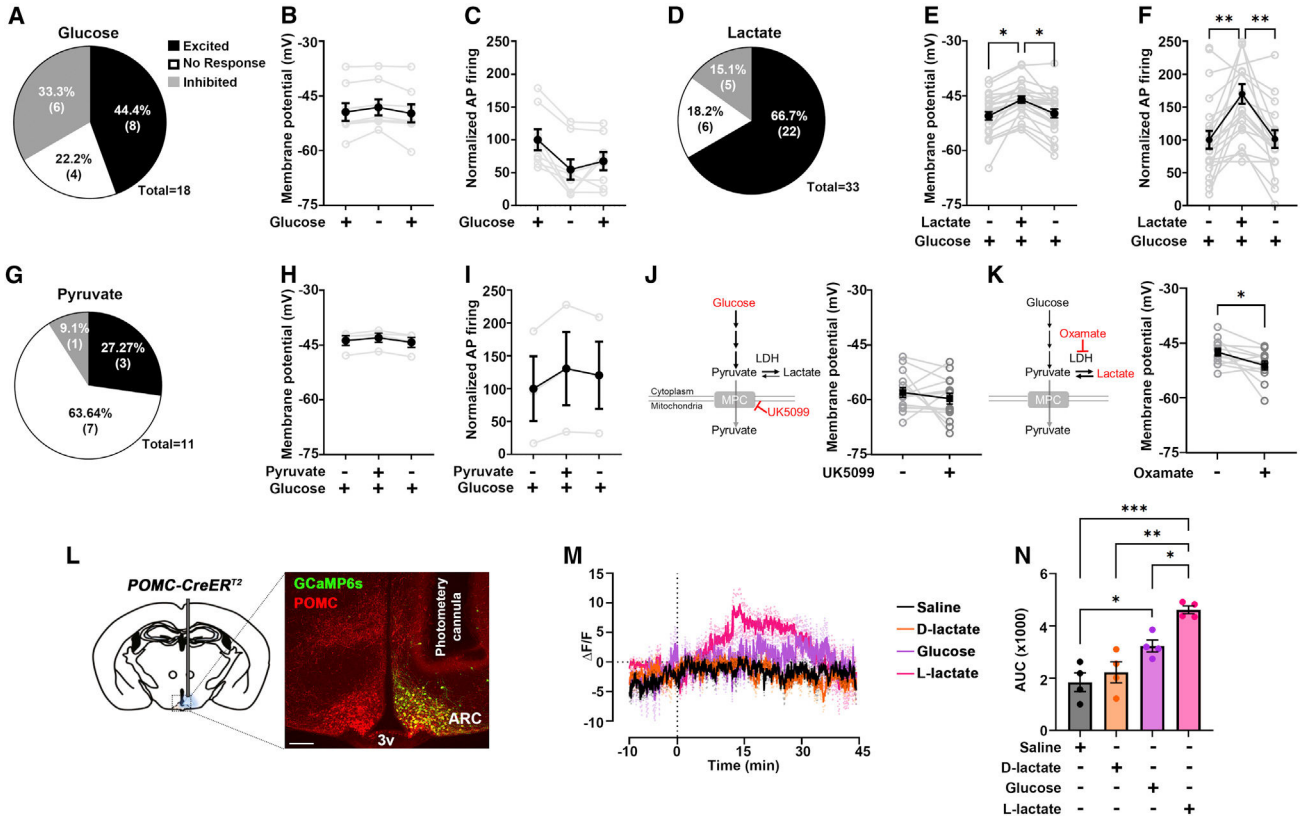

Figure 1. Addition of lactate activates a large population of POMC neurons

(A) Perforated patch recordings of hypothalamic POMC neurons exposed to physiological glucose levels (2.5 mM) using Pomc-*CreER*^{T2}; tdTomato mice (n = 18 neurons).

(B and C) Changes in POMC membrane potentials (B) and frequency of action potentials (C) recorded from POMC-tdTomato-positive neurons (n = 18) exposed to 2.5 mM glucose.

(D) Perforated patch recordings of hypothalamic POMC neurons exposed to physiological glucose levels (2.5 mM) and lactate (2 mM) using *Pomc-CreER*^{T2}; tdTomato mice (n = 33 neurons).

(E and F) Changes in POMC membrane potentials (E) and frequency of action potentials (F) recorded from POMC-tdTomato-positive neurons (n = 18) exposed to 2.5 mM glucose and 2 mM lactate.

(G) Perforated patch recordings of hypothalamic POMC neurons exposed to physiological glucose levels (2.5 mM) and pyruvate (2 mM) using *Pomc-CreER*^{T2}; tdTomato mice (n = 11 neurons).

(H and I) Changes in POMC membrane potentials (H) and frequency of action potentials (I) recorded from POMC-tdTomato-positive neurons (n = 18) exposed to 2.5 mM glucose and 2 mM pyruvate.

(J) Schematic and graph showing the effect of bath addition of UK5099 (5 μM) on POMC neurons membrane potential (n = 16).

(K) Schematic and graph showing the effect of bath addition of oxamate (6 mM) on POMC neuron membrane potential (n = 12). Electrophysiological responses were measured across 8–24 mice, and analyses were performed using one-way ANOVA and two-tailed t test.

(L) Schematic of the fiber photometry approach (left) and a coronal section from an rAAV-GCaMP6s-injected *Pomc-CreER*^{T2} mouse (right) showing the path of optical fiber and the injection site. The scale bar represents 200 μm.

(M) Average of normalized arcuate nucleus (ARC) POMC neuronal calcium signals in mice treated with either saline, glucose (i.c.v., 2.5 mM; M), D-lactate (i.c.v., 2 mM, N), or L-lactate (i.c.v., 2 mM; N) (n = 4 mice/group).

(N) The area under the curve (AUC) quantification of the GCaMP6s fluorescent signal increase over baseline during the overtime period in mice treated with either saline, glucose (i.c.v., 2.5 mM; M), D-lactate (i.c.v., 2 mM, N), or L-lactate (i.c.v., 2 mM; N) (n = 4 mice/group).

All data are shown as mean ± SEM. *p < 0.05; **p < 0.01; ***p < 0.001 by two-tailed t test. See also Figure S1.

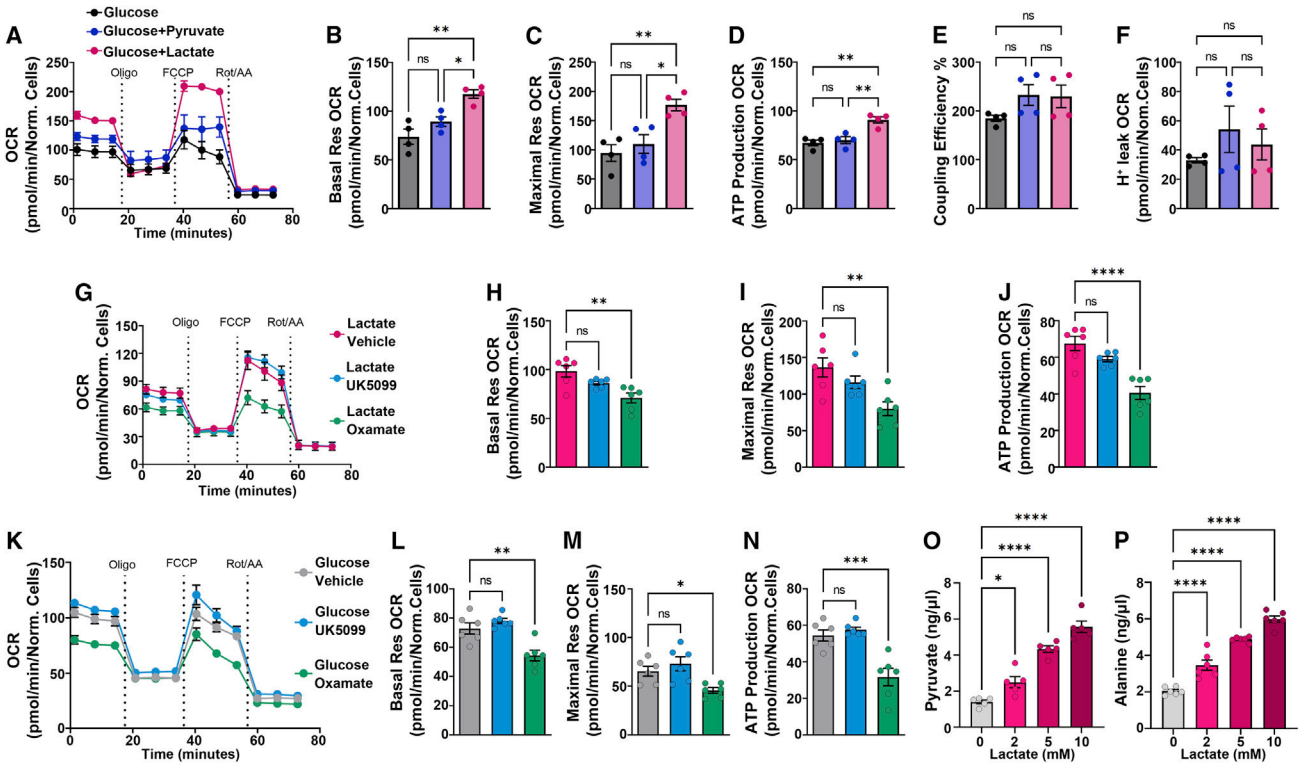

Figure 2. Inhibition of lactate dehydrogenase (LDH) reduces lactate-induced mitochondria respiration in primary mediobasal hypothalamic neuronal cells

(A–F) Graph showing mitochondrial oxygen consumption rate (OCR) levels induced by glucose (2.5 mM), glucose plus pyruvate (2.5 and 2 mM, respectively), or glucose plus lactate (2.5 and 2 mM, respectively) (A) in basal (B) and maximal respiration (C), ATP production (D), coupling efficiency (E), and proton leak (F).

(G–J) Graph showing OCR levels induced by glucose plus lactate (2.5 and 2 mM, respectively) after addition of UK5099 (5 µM) or oxamate (6 mM) (G) in mitochondrial basal (H) and maximal respiration (I) and ATP production (J).

(K–N) Graph showing OCR levels induced by glucose (2.5 mM) after addition of UK5099 (5 µM) or oxamate (6 mM) (K) in basal (L) and maximal respiration (M) and ATP production (N).

(O and P) Extracellular pyruvate (O) and alanine (P) were measured in primary mediobasal hypothalamic neuronal cultures media after increasing lactate concentrations. Mitochondria respiration measurements and lactate assays were measured in n = 4–6 per group across mouse primary mediobasal hypothalamic neuronal cells derived from *Pomc-CreER^{T2}*; tdTomato mice (n = 8).

All data are shown as mean ± SEM. ns, not significant; *p < 0.05; **p < 0.01; ***p < 0.001; ****p < 0.0001 by one-way ANOVA.

See also Figures S2 and S3.

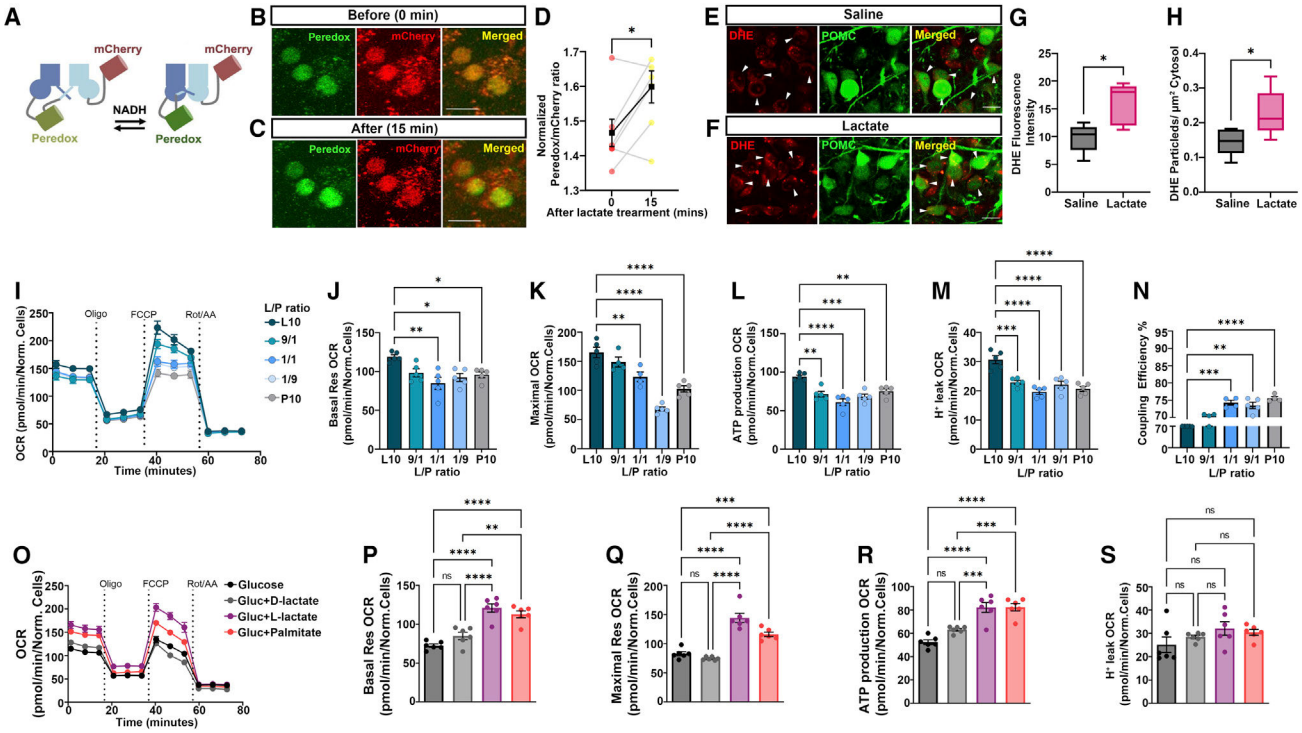

Figure 3. Lactate administration alters the redox state of POMC neurons

(A) Schematic illustration of the variation of the fluorescent signal after NADH binding to Peredox.

(B and C) Fluorescent images by 2-photon microscopy showing Peredox (green) in POMC neurons (labeled with mCherry) at 0 (B) and 15 min (C) after 2 mM lactate administration to the bath (containing 2.5 mM glucose) containing hypothalamic section. The scale bars represent 20 μm.

(D) Graph showing the measurement of the fluorescent signal of Peredox in POMC neurons at 0 and 15 min after 2 mM lactate administration to the bath (containing 2.5 mM glucose) in hypothalamic sections.

(E and F) Representative fluorescent micrographs showing DHE labeling (red) in POMC neurons (green) in mouse brain after saline (E) lactate (2 mM) (F) administration (i.c.v.). The scale bars represent 20 μm.

(G and H) Graphs showing DHE measurement as fluorescent intensity (G) or as number of particles per μm^2 of POMC cytosol (H).

(I–N) Graphs showing mitochondrial OCR (I) in basal (J) and maximal (K) respiration, ATP production (L), proton leak (M), and percentage of coupling efficiency (N) under different lactate/pyruvate ratios of primary mediobasal hypothalamic neuronal cell cultures.

(O–S) Graphs showing mitochondrial OCR in primary mediobasal hypothalamic neuronal cell cultures treated with glucose alone, glucose plus D-lactate, glucose plus L-lactate, and glucose plus palmitate (O) in basal (P) and maximal (Q) respiration, ATP production (R), and proton leak (S) of primary mediobasal hypothalamic neuronal cell cultures.

All data are shown as mean ± SEM. ns, not significant; *p < 0.05; **p < 0.01; ***p < 0.001; ****p < 0.0001 by one-way ANOVA and two-tailed t test.

See also Figure S3.

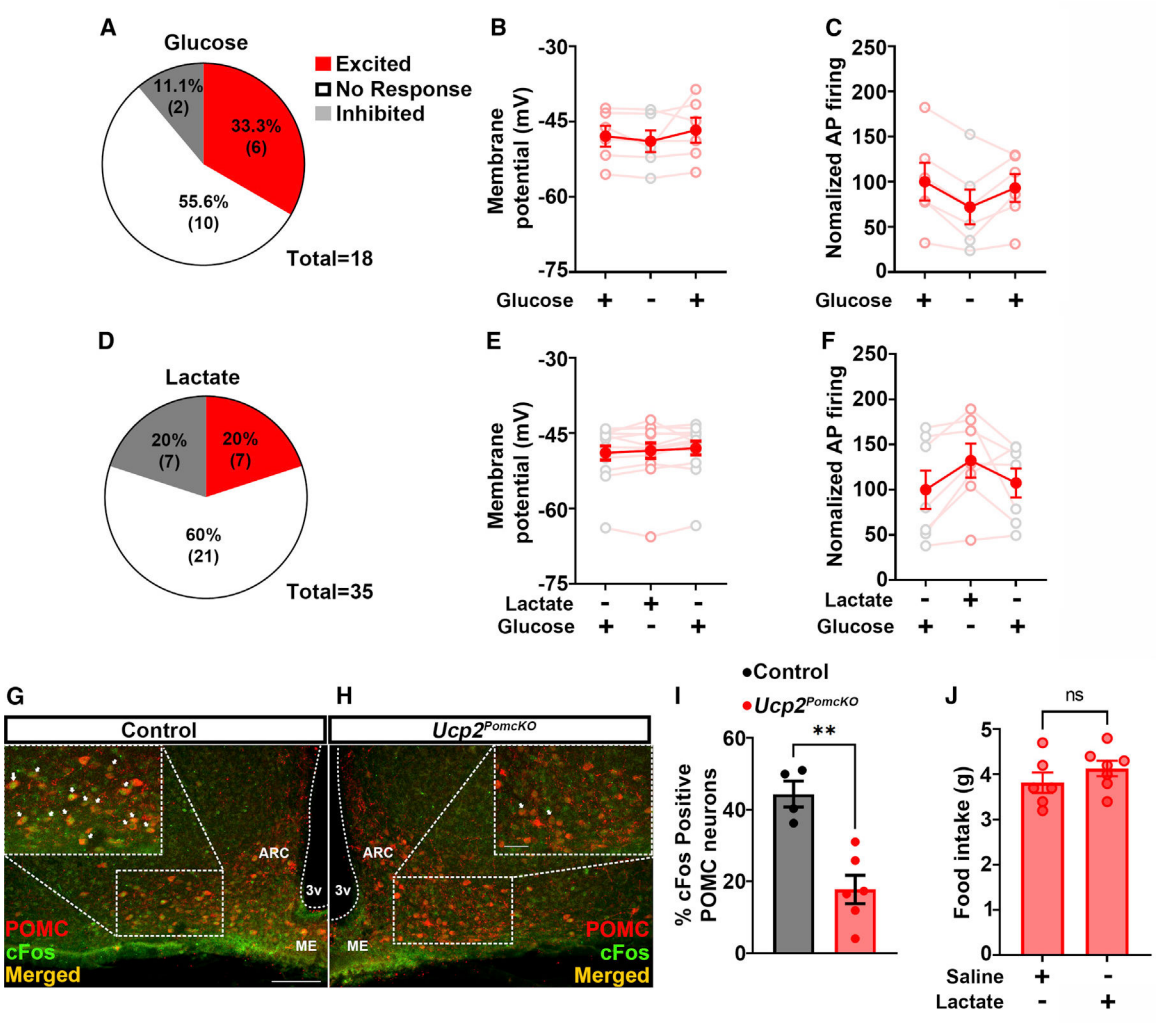

Figure 4. Lactate-induced POMC neuronal activation is impaired in *Ucp2*^{PomcKO} mice

(A) Perforated patch recordings of hypothalamic POMC neurons exposed to physiological glucose levels (2.5 mM) in *Ucp2*$^{fl/fl}$; Pomc-*CreER*^{T2}; tdTomato (*Ucp2*^{PomcKO}) mice (n = 18 neurons/11 mice).

(B and C) Changes in POMC membrane potentials (B) and frequency of action potentials (C) recorded from POMC-tdTomato-positive neurons (n = 17) of *Ucp2*^{PomcKO} mice exposed to 2.5 mM glucose.

(D) Perforated patch recordings of hypothalamic POMC neurons in *Ucp2*^{PomcKO} mice (n = 35 neurons/27 mice) exposed to physiological glucose levels (2.5 mM) and lactate (2 mM).

(E and F) Changes in POMC membrane potentials (E) and frequency of action potentials (F) were recorded from POMC-tdTomato-positive neurons (n = 14) of *Ucp2*^{PomcKO} mice exposed to 2.5 mM glucose and 2 mM lactate in the bath.

(G and H) Representative hypothalamic sections were stained for POMC (red) and cFos (green) from a control (G) and a *Ucp2*^{PomcKO} mouse (H) sacrificed 1 h after lactate (i.c.v., 2 mM) administration. Scale bars in (G) and (H) represent 100 and 50 μm, respectively.

(I) Graph showing the percentage of cFos-positive POMC neurons in control (n = 5) and *Ucp2*^{PomcKO} mice (n = 6) 1 h after lactate (i.c.v., 2 mM) administration.

(J) Graph showing cumulative 24 h of food intake of $Ucp2^{PomcKO}$ mice treated either with vehicle (saline) or lactate.

All data are shown as mean ± SEM. ns, not significant; **p < 0.01 by one-way ANOVA and two-tailed t test.

See also Figure S4.

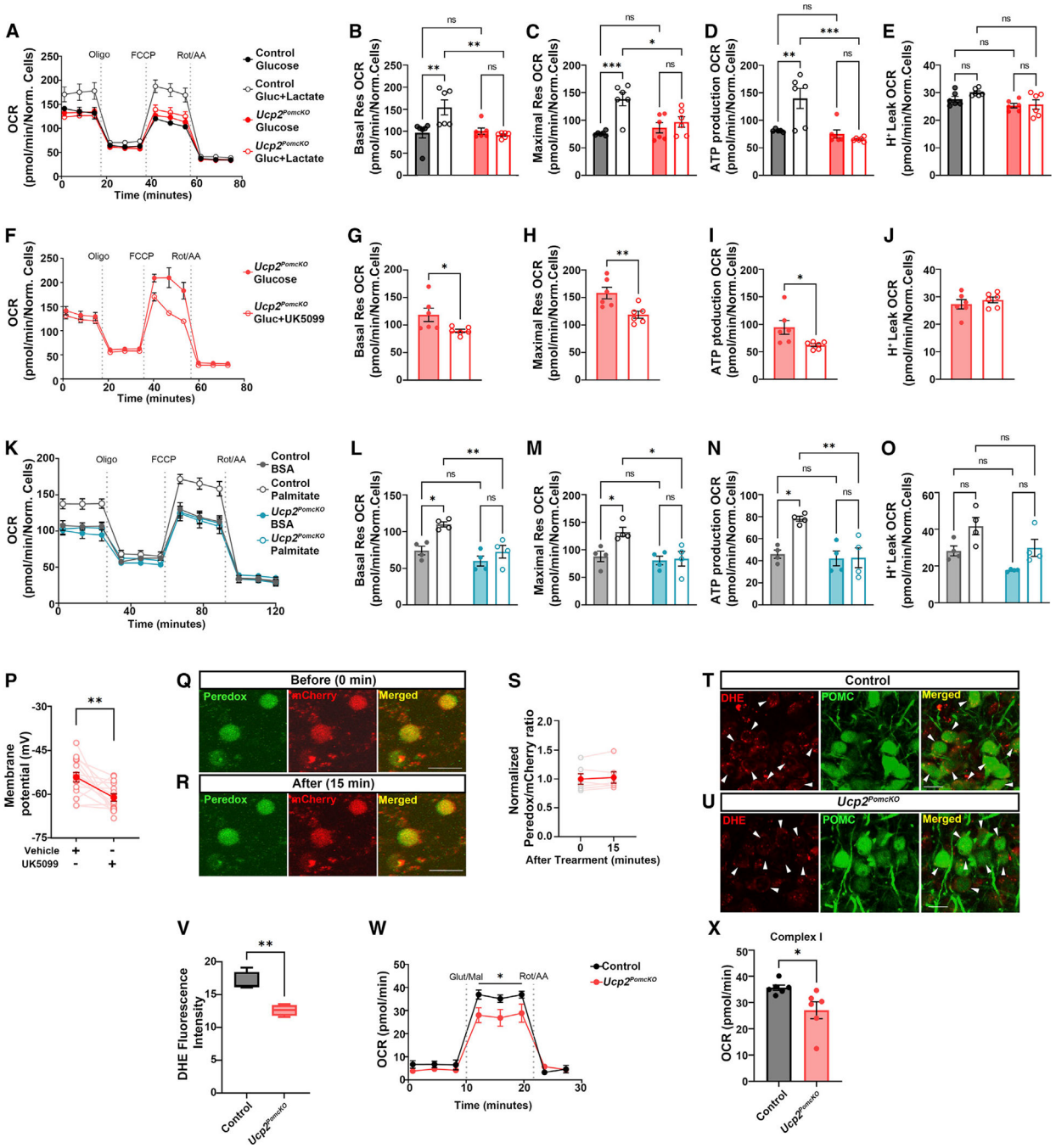

Figure 5. Lactate-induced mitochondrial respiration is impaired in *Ucp2*^{PomcKO} mice

(A–E) Graph showing mitochondrial OCR levels induced by glucose (2.5 mM) or glucose plus lactate (2.5 and 2 mM, respectively) administration in basal (B) and maximal respiration (C), ATP production (D), and proton leak (E) induced by glucose (2.5 mM) or glucose plus lactate (2.5 and 2 mM, respectively) to primary mediobasal hypothalamic neuronal cell cultures from control and *Ucp2*^{PomcKO} mice (n = 6/group).

(F–J) Graphs showing mitochondrial OCR (F) in basal (G) and maximal respiration (H), ATP production (I), and proton leak (J) induced by glucose (2.5 mM) or glucose

plus UK5099 (5 μM) in primary mediobasal hypothalamic neuronal cell cultures from *Ucp2*^{PomcKO} mice (n = 6/group).

(K–O) Graphs showing mitochondrial OCR (K) in basal (L) and maximal respiration (M), ATP production (N), and proton leak (O) induced by glucose (2.5 mM) or glucose plus BSA (33.3 μM) or glucose plus palmitate (200 μM) in primary mediobasal hypothalamic neuronal cell cultures from control and *Ucp2*^{PomcKO} mice (n = 4–5/group).

(P) Graph showing POMC membrane potential in *Ucp2*^{PomcKO} mice (n = 15 neurons/10 mice) under 2.5 mM glucose condition treated either with vehicle or UK5099 (5 μM).

(Q and R) fluorescent images by 2-photon microscopy showing Peredox (green) in POMC neurons (red) from a hypothalamic section of an *Ucp2*^{PomcKO} mouse at 0 (Q) and 15 min (R) after addition of 2 mM lactate in 2.5 mM glucose containing bath. Scale bar represents 20 μm.

(S) Graph showing the measurement of the Peredox fluorescent signal in POMC neurons (n = 12 cells/6 mice) of *Ucp2*^{PomcKO} mice at 0 and 15 min after lactate addition to the glucose-containing bath.

(T and U) Representative fluorescent micrographs showing DHE labeling (red) in POMC neurons (green) in a control (T) and a *Ucp2*^{PomcKO} mouse (U) after lactate administration (i.c.v., 2 mM). Scale bar represents 20 μm.

(V) Graph showing DHE fluorescent intensity of POMC cytosol in control and *Ucp2*^{PomcKO} mice (n = 4).

(W and X) Graphs showing glutamate/malate-induced mitochondrial respiration (W), representative of the ETC complex I activity (X), in primary mediobasal hypothalamic neuronal cell cultures from control and *Ucp2*^{PomcKO} mice (n = 8).

All data are shown as mean ± SEM. ns, not significant; *p < 0.05; **p < 0.01; ***p < 0.001 by two-way ANOVA and two-tailed t test.

See also Figure S5.

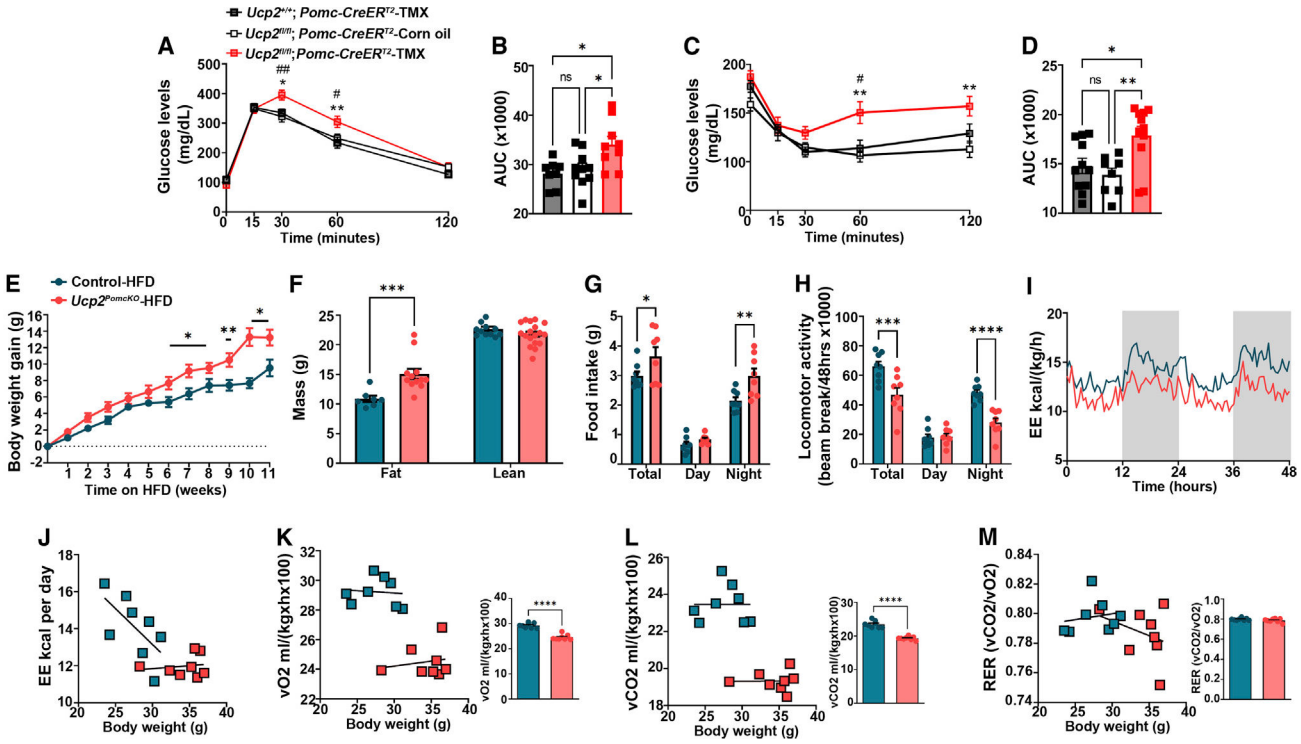

Figure 6. *Ucp2*^{PomcKO} mice are glucose intolerant and prone to diet-induced obesity

(A and B) Graphs showing changes in blood glucose levels (A) and the AUC (B) during glucose-tolerance tests in controls (*Ucp2*$^{+/+}$; *Pomc-CreER*^{T2}-TMX [n = 8] and *Ucp2*$^{fl/fl}$; Pomc-CreERT2-corn oil [n = 10]) and *Ucp2*^{PomcKO} mice (*Ucp2*$^{fl/fl}$; Pomc-CreERT2-TMX; n = 10).

(C and D) Graphs showing changes in blood glucose levels (C) and AUC (D) during insulin-tolerance tests in controls (*Ucp2*$^{+/+}$; *Pomc-CreER*^{T2}-TMX [n = 8] and *Ucp2*$^{fl/fl}$; Pomc-CreERT2-corn oil [n = 11]) and *Ucp2*^{PomcKO} mice (*Ucp2*$^{fl/fl}$; Pomc-CreERT2-TMX; n = 11). Data are presented as mean ± SEM. $^{\#}p < 0.05$; $^{\#\#}p < 0.01$ for *Ucp2*$^{fl/fl}$; Pomc-CreERT2-corn oil versus *Ucp2*$^{fl/fl}$; Pomc-CreERT2-TMX; ns, not significant; *p < 0.05; **p < 0.01 for *Ucp2*$^{+/+}$; *Pomc-CreER*^{T2}-TMX versus *Ucp2*$^{fl/fl}$; Pomc-CreERT2-TMX by two-way ANOVA and one-way ANOVA.

(E and F) Graphs showing body weight gain (E) and body composition (11 week of high-fat diet [HFD]) (F) in control and *Ucp2*^{PomcKO} mice exposed to HFD (n = 7–11/group).

(G) Graph showing 24 h cumulative food intake in control and *Ucp2*^{PomcKO} mice exposed to 11 weeks of HFD (n = 8/group).

(H) Graph showing locomotor activity of control and *Ucp2*^{PomcKO} mice exposed to 11 weeks of HFD (n = 8/group).

(I and J) Graphs showing energy expenditure of control and *Ucp2*^{PomcKO} mice exposed to 11 weeks of HFD (n = 8/group).

(K–M) Graphs showing VO_2 consumed (K), CO_2 produced (L), and their ratio (RER; M) in control and *Ucp2*^{PomcKO} mice exposed to 11 weeks of HFD (n = 8/group).

Data are shown as mean ± SEM. *p < 0.05; **p < 0.01; ***p < 0.001; ****p < 0.0001 by two-way ANOVA and two-tailed t test.

See also Figure S6.

Table 1.

Hypercarb column chromatographic separation

Time	%A	%B
0	100	0
1	100	0
12	20	80
14	20	80
14.1	100	0
18.1	100	0

Table 2.

Kinetex F5 column chromatographic separation

Time	%A	%B
0	100	0
0.5	100	0
15	0	100
16	0	100
16.1	100	0
20	100	0

KEY RESOURCES TABLE

REAGENT or RESOURCE	SOURCE	IDENTIFIER
Antibodies		
POMC	Phoenix Pharmaceuticals	Cat# H-029-30; RRID: AB_2307442
c-Fos	Santa Cruz Biotechnology	Cat# sc-52; RRID: AB_2106783
Alexa 488 donkey anti-rabbit	Thermo Fisher Scientific	Cat# A21206; RRID:AB_2535792
Alexa 594 goat anti-rabbit	Thermo Fisher Scientific	Cat# A32740; RRID:AB_2762824
Alexa 488 goat anti-mouse	Thermo Fisher Scientific	Cat# A32723; RRID:AB_2633275
Alexa 488 goat anti-chicken	Thermo Fisher Scientific	Cat# A11039; RRID:AB_142924
Peroxidase conjugated anti-DIG	Sigma-Aldrich	Cat# 11207733910; RRID:AB_514500
Donkey anti-rabbit IgG	Jackson ImmunoResearch	Cat# 711-005-152; RRID:AB_2340585
HA .11	BioLegend	Cat# 901513; RRID:AB_2565335
GFP	Abcam	Cat# ab13970; RRID:AB_300798
Bacterial and virus strains		
pcDNA3.1-Peredox-mCherry-NLS	Addgene	Cat# 32384
AVV2-CMV-DIO-Peredox-mcherry-NLS	Vector Biolabs	This paper
pAAV.Syn.Flex.GCaMP6s.WPRE.SV40	Addgene	Cat#100845-AAV9
Chemicals, peptides, and recombinant proteins		
Tamoxifen	Sigma-Aldrich	Cat# T5648
Corn Oil	Sigma-Aldrich	Cat# C8267
4-hydroxytamoxifen	Sigma-Aldrich	Cat# H7904
Hibernate-A Medium	Thermo Fisher Scientific	Cat# A1247501
Poly-D-lysine	Sigma-Aldrich	Cat# P6407
Neurobasal-A medium	Thermo Fisher Scientific	Cat# 10888022
B-27 Supplement	Thermo Fisher Scientific	Cat# 17504044
GlutaMAX-I	Thermo Fisher Scientific	Cat# 35050061
CultureOne supplement	Thermo Fisher Scientific	Cat# A3320201
T3 RNA polymerase	Promega	Cat# P2083
Vectashield mounting solution	Vector Laboratories	Cat# H-1000
DAPI	Thermo Fisher Scientific	Cat# P36962
Heparin	Sigma-Aldrich	Cat# H3393
Anti-HA coated Magnetic Beads	Thermo Fisher Scientific	Cat# 88836
Seahorse XF Base medium	Agilent Technologies	Cat# 102353-100
Glucose	Sigma-Aldrich	Cat# 7021

REAGENT or RESOURCE	SOURCE	IDENTIFIER
D-lactate	Sigma-Aldrich	Cat# 71716
L-lactate	Sigma-Aldrich	Cat# L7022
Pyruvate	Sigma-Aldrich	Cat# P2256
Palmitate	Sigma-Aldrich	Cat# P9767
UK5099	Sigma-Aldrich	Cat# PZ0160
Oxamate	Sigma-Aldrich	Cat# O2751
2 Deoxy D-glucose	Sigma-Aldrich	Cat# D8375
Oligomycin	Sigma-Aldrich	Cat# 495455
Carbonyl cyanide-p-(trifluoromethoxy)phenylhydrazone	Sigma-Aldrich	Cat# C2920
Antimycin A	Sigma-Aldrich	Cat# A8674
Rotenone	Sigma-Aldrich	Cat# R8875
Dihydroerhidium	Thermo Fisher Scientific	Cat# D11347
Insulin	Eli Lilly and company).	Humulin R
Critical commercial assays		
Qiagen RNeasy Plus Micro Kit	Qiagen	Cat# 74034
High Capacity cDNA Reverse transcription Kit	Thermo Fisher Scientific	Cat# 4368814
DIG RNA labeling Mix	Sigma-Aldrich	Cat# 11277073910
TaqMan PreAmp Master Mix	Thermo Fisher Scientific	Cat# 4391128
L-lactate assay kit	Abcam	Cat# ab65331
Deposited data		
Metabolomics	http://dev.metabolomicsworkbench.org:22222/data/DRCCMetadata.php?Mode=Study&StudyID=ST002361&Access=FdhW7067; https://doi.org/10.21228/M8R12T	https://doi.org/10.21228/M8R12T
Experimental models: Organisms/strains		
B6;129S-Ucp2$^{tm2.1Lowl/J}$	Jackson Laboratory	Stock # 022394
POMC-cre:ERT2; tdTomato	Berglund et al.[30]	N/A
Ucp2fl/flPOMC-Cre:ERT2	This paper	N/A
B6N.129-*Rpl22tm1.1Psam/J*	Jackson Laboratory	Stock #011029
POMC-cre:ERT2; Rpl HA/HA	This paper	N/A
Ucp2fl/flPOMC-cre:ERT2; Rpl HA/HA	This paper	N/A
Oligonucleotides		
TaqMan Cpt1a	Thermo Fisher Scientific	Assay ID Mm01231183_m1
TaqMan Cpt1b	Thermo Fisher Scientific	Assay ID Mm00487191_g1
TaqMan Cpt1c	Thermo Fisher Scientific	Assay ID Mm00463970_m1
TaqMan Cpt2	Thermo Fisher Scientific	Assay ID Mm00487205_m1
TaqMan Pomc	Thermo Fisher Scientific	Assay ID Mm00435874_m1
TaqMan Ldha	Thermo Fisher Scientific	Assay ID Mm01612132_g1

REAGENT or RESOURCE	SOURCE	IDENTIFIER
TaqMan Ldhb	Thermo Fisher Scientific	Assay ID Mm00485106_m1
TaqMan Ucp2	Thermo Fisher Scientific	Assay ID Mm00627599_m1
TaqMan Got1	Thermo Fisher Scientific	Assay ID Mm01195792_g1
TaqMan Got2	Thermo Fisher Scientific	Assay ID Mm00494703_m1
TaqMan Mdh1	Thermo Fisher Scientific	Assay ID Mm00485106_m1
TaqMan Mdh2	Thermo Fisher Scientific	Assay ID Mm00725890_s1
TaqMan Actb	Thermo Fisher Scientific	Assay ID Mm02619580-g1
TaqMan Actb	Thermo Fisher Scientific	Cat# 4352341E
Software and algorithms		
Seahorse Wave Controller Software 2.6	Agilent Technologies software	Wave 2.6.0, https://www.agilent.com/en/product/cell-analysis/real-time-cell-metabolic-analysis/xf-software/seahorse-wave-controller-software-2-6-1-740904
ImageJ	National Institutes of Health	1.47v
Prism 9.03 software	GraphPad Software	https://www.graphpad.com/scientific-software/prism/
El-MAVEN and Polly software	Elucidata	N/A
MATLAB	MATLAB	https://es.mathworks.com/products/matlab-online.html
Other		
Fluorescence Microscope	KEYENCE	Model BZ-X710
Fiber photometry processor	Tucker Davis Technologies	RZ10x, https://www.tdt.com/component/rz10x-processor/
Electron microscope	Philips	CM-10
Glucometer	Bayer	Contour 9556c
Seahorse XFe 96 Analyzer	Agilent Technologies	XF Analyzers
2 photon microscope	LaVision Biotec	LaVision TriM Scope II
XF96 cell culture microplates	Agilent Technologies	Cat# 101085-004
ICV cannula	P1 Technologies	33 gauge
Fiber-optic cannula	Doric Lenses Inc	MFC_400/430-0.48_7 mm_MF1.25_FLT
Microvette CB 300 K2 EDTA	Sarstedt	Cat# 16.444.100
Glass capillary	World precision instruments	Cat# 1B100F-6
6600 Triple TOF LC-MS/MS mass spectrometer	Sciex	N/A
Hypercarb column (3 μm particle size, 4.6 × 100 mm)	Thermo Fisher Scientific	35003-104630